X-612-69-258
PREPRINT

SOLAR PROTON OBSERVATIONS 1-10 MEV

D. J. WILLIAMS

JUNE 1969

GSFC

GODDARD SPACE FLIGHT CENTER
GREENBELT, MARYLAND

X-612-69-258

SOLAR PROTON OBSERVATIONS, 1-10 MEV*

D. J. Williams

June 1969

NASA-GODDARD SPACE FLIGHT CENTER

Greenbelt, Maryland

*Invited paper presented at the "Seminar on the Study of Interplanetary Space Physics using Cosmic Rays" USSR Academy of Sciences, June 4-7, 1969, Leningrad, USSR. Proceedings to be published by A. I. Ioffe Physical Technical Institute, Academy of Sciences, USSR, 1969.

SOLAR PROTON OBSERVATIONS, 1-10 MEV*

D. J. Williams

ABSTRACT

A brief resume of diffusion models and solar proton propagation in the interplanetary medium is given. Observations of solar protons from the Solar Proton Monitoring Experiment flown aboard the Explorer 34 satellite are then presented. Attention is focused on the 1-10 Mev proton intensities and their different behavioral characteristics as compared to higher energy (> few tens of Mev) solar protons. Observations of quasi-periodic variations in the 1-10 Mev proton intensities are presented. Power spectra are shown for both quiet and active periods. It is found that during the quiet periods analyzed, the 1-10 Mev proton intensity power spectra displayed an f^{-1} to $f^{-1.5}$ trend. Some mechanism is apparently ordering the proton intensities in the frequency domain. Active periods are shown in which prominent peaks in the power spectra are observed at 0.0125 cycles per minute ($2.1\ (10)^{-4}$ Hz; 80 minute period) and at 0.02 cycles per minute ($3.3\ (10)^{-4}$ Hz; 50 minute period). A summary of observations concerning the entry of low energy protons into the magnetosphere is given. It is argued that the entry of these particles into the magnetosphere is governed by the existing magnetosphere configuration. As this configuration is in turn determined by the boundary conditions imposed by the interplanetary medium, it is further argued that changes in the mode of entry should be expected as interplanetary conditions change. Data indicative of both diffusive and direct entry are reviewed.

---

*Invited paper presented at the "Seminar on the Study of Interplanetary Space Physics using Cosmic Rays" USSR Academy of Sciences, June 4-7, 1969, Leningrad, USSR. Proceedings to be published by A. I. Ioffe Physical Technical Institute, Academy of Sciences, USSR, 1969.

CONTENTS

SOLAR PROTON OBSERVATIONS, 1-10 MEV

INTRODUCTION

In this report we present observations of solar protons recorded by the Solar Proton Monitoring Experiment (SPME) onboard Explorer 34. We shall emphasize the lower energy (~1 Mev) observations and will discuss i) propagation in the interplanetary medium and the general characteristics of the low energy solar proton population as compared with higher energies, ii) observations of quasi-periodic variations in the low energy solar proton intensities, and iii) the entry of these protons into the magnetosphere.

Explorer 34 was launched on May 24, 1967 into a highly elliptic orbit having a ~34.5 R_E apogee, a 67° inclination and a period of ~4.3 days. The satellite was spin stabilized at 22.4 revolutions per minute with its spin axis oriented perpendicular (90° ± 2°) to the ecliptic plane. After nearly two years of operation Explorer 34 entered the earth's atmosphere on May 3, 1969.

The SPME consists of four basic detecting channels measuring protons ≥ 60 Mev, ≥ 30 Mev, ≥ 10 Mev, and 1-10 Mev. All channels employ solid state detectors and use a combination of discriminator levels and shielding thicknesses to obtain the above proton sensitivities. The channels also respond to alpha particles of energy roughly four times the quoted proton sensitivity. Electron contamination is negligible in all channels except the ≥ 10 Mev channel, whose primary electron response is in the radiation belts.

The ≥ 60 Mev and ≥ 30 Mev channels are omnidirectional over 2π steradians and have an effective area of ~ 1 cm^2. The ≥ 10 Mev channel is also omnidirectional over 2π steradians and has an effective area of 0.13 cm^2. Data from these three channels are used to produce nearly continuous monitoring observations of solar protons. These observations are routinely published in the Solar-Geophysical Bulletin in the form of both plots and tabulations of the hourly flux averages for the month six months before publication [Solar Geophysical Bulletin, 1968].

The 1-10 Mev channel has a 60° full look angle, uses an 86 micron thick surface barrier solid state detector with a 2 cm^2 area, and is oriented to look out normal to the satellite spin axis. Since this channel accumulates for several revolutions of the satellite, no directional information in the ecliptic plane is obtained. However rough directional information with respect to the local magnetic field may be obtained by observing this field direction move in and out of the detector look angle.

GENERAL CONSIDERATIONS

Applications of simple three-dimensional isotropic diffusion theory to the propagation of solar cosmic rays (Morrison, 1956; Parker, 1956, 1963; Meyer et al, 1956; Bryant et al, 1962; Hoffman and Winckler, 1963; Krimigis, 1965) have been able to describe energetic ($\geq$ few tens of Mev) solar proton time histories as observed at ~ 1 AU only in the isotropic phase near and somewhat beyond the time of maximum intensity of a solar particle event (see for example reviews of

solar cosmic ray observations by Webber, 1963, Fichtel and McDonald, 1967 and Kavanaugh et al, 1969). In spite of their limited success, these early studies uncovered new insights in the understanding of energetic particle propagation in the interplanetary medium. However, they are now known to be unable to explain certain important characteristics in the time histories of solar flare protons as observed at $\sim$1 AU. For example, isotropic diffusion theory is unable to account for a) observed aniosotropic angular distributions in the near-earth solar proton intensities (Lüst and Simpson, 1957; McCracken, 1962; Bartley et al, 1966; Fan et al, 1966) and b) the dependence of the arrival time, the rise time to maximum intensity, and the shape of the intensity time curve on the solar longitude of the parent flare (west longitude flares are observed to yield faster arrival and rise times at $\sim$1 AU than east longitude flares (Burlaga, 1967)).

Given these facts plus the existence of a spiral interplanetary magnetic field (Parker, 1958) it became apparent that if diffusive processes between the earth and the sun were responsible for the near-earth solar proton intensities and time histories, they must be anisotropic in character. Further, the strong coupling between charged particles and magnetic fields would indicate that the principal axes of diffusion should lie along and perpendicular to the local magnetic field line. Direct observations of the strong collimation of solar protons along interplanetary field lines have been reported by McCracken and Ness (1966).

The results of several studies (Reid, 1964; Axford, 1965, Roelof, 1966; Jokipii, 1966; Burlaga, 1967; Dolginov and Toptygin, 1967) have produced a

picture of aniosotropic diffusion of energetic solar protons through the interplanetary medium which far better fits the observations than the earlier isotropic diffusion studies. Spatially anisotropic diffusion is able to qualitatively account for item a) above and quantitatively account for item b). However some questions still remain as to whether diffusion effects within ~ 1 AU are primarily responsible for the solar proton characteristics observed near the earth. One reason for this concern is that two different models (Reid (1964)—Axford (1965), and Burlaga, (1967)) of solar proton release into and propagation through the interplanetary regions yield similar and satisfactory fits to the intensity-time observations, thereby eliminating for the time being any uniqueness in a diffusive solution to the problem. Also, while the models do predict different anisotropy versus time profiles, they can at best only indicate the trend of possible large anisotropies in the solar proton angular distributions - i. e., they are generally qualitative in accounting for such anisotropies. In particular, the observed large anisotropies lasting beyond the maximum of an event (McCracken, 1962; McCracken et al, 1967) cannot be explained by a pure diffusive process.

Complimentary to the model studies, Roelof (1966) and Jokipii (1966) have conducted detailed investigations on a specific scattering mechanism which may be responsible for the anisotropic diffusive characteristics of energetic solar proton time histories. They have used random interplanetary magnetic field irregularities in a particle pitch-angle scattering formalism and have obtained the components of the diffusion tensor in terms of the power spectrum of the field

irregularities. Roelof (1966) has shown that these results allow for both collimation and diffusive effects and depend directly on the magnitude and spatial dependences of the power spectrum. In fact, in the case where pitch-angle scattering is effective for a large distance along the field line, Roelof (1966) has shown that in a spiral interplanetary field configuration (Parker, 1958) the one-dimensional anisotropic diffusion equation obtained from such a pitch-angle scattering process has the same functional form as the three-dimensional isotropic equation proposed earlier (Parker, 1963) and thus must duplicate its successes as well as rectify some of its deficiencies.

It is important to resolve the ambiguities in the physical model of the injection and propagation region since the characteristics of the region directly enter the calculations of the diffusion coefficient as described above. Conversely, it is possible that the results of the calculations of particle transport in disordered magnetic fields can be used to infer some of the local and large scale characteristics of the interplanetary magnetic field (Roelof, 1966; Jokipii, 1966).

The preceding remarks have applied mainly to energetic ($\geq$ few tens of Mev) solar protons. As observations have extended to lower energies the spatial and temporal complexity of the events has greatly increased. For example, recurrence events are seen where low energy solar protons, contained within a solar longitude interval of several tens of degrees, are observed to recur with a 27-day period (Bryant et al, 1965; Fan et al, 1966). The nature of these recurring events has led to the suggestion of particle storage near the sun above

the active center (Fichtel and McDonald, 1967). Particle storage at the sun has also been used to explain observed anisotropies and durations of solar electron events (Lin and Anderson, 1967) and to explain the observed "core-halo" structure present in certain events (Lin et al, 1968; Anderson, 1968).

The existence of rapid low energy proton propagation transverse to the field lines has been argued from the observation of early particle onset times near the earth from flares far removed in solar longitude from the field line connecting to the near-earth region (McCracken et al, 1967; Williams and Bostrom, 1967), and from measurements of event onsets at interplanetary positions separated by longitude intervals up to 180° (Fan et al, 1968).

Observations of low energy ($\sim$ 1 Mev) solar protons have also shown that non-flare associated events are present in the interplanetary medium for a significant fraction of the time, even during solar minimum (Krimigis and Van Allen, 1966). In addition, the time structure displayed by the low energy solar protons is in general not at all indicative of a diffusive process (see for example, Fan et al, 1966 and Figures 1-3 of this paper). It has also been observed that the lower energy solar protons are at times very strongly collimated and flow along interplanetary magnetic field filaments (McCracken and Ness, 1966; McCracken et al, 1968). However, in a later section of this note we shall see cases where the low energy solar proton intensities are roughly isotropic and thus independent of the local magnetic field direction (McCracken et al, 1968).

To illustrate some of the more general solar proton characteristics we show in Figures 1, 2, and 3 hourly averages of the four SPME detecting channels for the time periods indicated.

Shown along with hourly average intensities are the radial distance from the center of the earth to Explorer 34 (apogee $\simeq 34.5\ R_E$) and the projection of the orbit on the ecliptic plane. The higher count rates at or near perigee are due to the earth's radiation belts. Note that this effect is particularly noticeable in the ≥ 10 Mev channel which has the largest electron sensitivity.

Figure 1 shows the active period of the May 1967 events, Figure 2 shows a period of moderate to light activity (June 1967) and Figure 3 shows a period of no observable activity in August 1967 in the ≥ 60 Mev and ≥ 30 Mev channels.

Figures 1, 2, and 3 clearly show the rapid increase of solar proton activity as lower energies are sampled. In addition it is clear that the 1-10 Mev solar proton time histories differ markedly from the ≥ 60 Mev, ≥ 30 Mev and ≥ 10 Mev time profiles. This qualitative difference in the 1-10 Mev and ≥ 10 Mev time profiles is so often characteristic of solar protons that it is indicative of a transition energy existing between 1 and 10 Mev which separates energy regimes responding to different acceleration and/or transport processes.

Figure 3 is shown as an example of the sudden appearance of a very soft solar proton spectrum. No intensity increase above background is observed at ≥ 30 Mev, a small increase (partially obscured by the radiation belts) is observed for ≥ 10 Mev protons, while the 1-10 Mev proton intensities increase by four

orders of magnitude over their earlier level. For a differential spectrum of the form $N(E)\,dE \propto E^{-n}$, Figure 3 yields values of n as large as 4.

In summary, the sun appears to be a prolific source of low energy ($\sim$ 1 Mev) protons. During periods of relatively weak solar activity, very soft proton spectra are often observed. This low energy ($\sim$ 1 Mev) portion of the solar proton spectrum also often exhibits a markedly different time structure at $\sim$ 1 AU than the higher energy ($\gtrsim$ 10 Mev) protons. It remains to be seen whether diffusive processes can reconcile these differences - particularly since there is even reason to question the effectiveness of a diffusion mechanism between the earth and the sun which controls the behavior of energetic ($\geq$ few tens of Mev) solar protons as observed at $\sim$ 1 AU.

QUASI-PERIODIC INTENSITY FLUCTUATIONS

Satellite observations of quasi-periodic fluctuations in solar proton intensities ranging in period from about 15 minutes to several hours have been reported by Bryant et al, (1965) and Fan et al, (1966). For the event of September 10, 1961 Bryant et al, (1965) show a sequence of variations obtained within the earth's magnetosheath which displayed a period of $\sim$ 90 minutes and constant phase over the entire energy range of 5.7 - 87 Mev. The coherency of the oscillations (lack of energy dispersion) led to the interpretation that they were controlled locally, i.e., near the region of observation.

Fan et al, (1966) suggested that the short term ($\sim$ 15 minute) intensity variations which they observed in interplanetary regions could be produced by field

modulation caused by the propagation of magnetohydrodynamic waves in the interplanetary medium. Using transversely propagating waves with a velocity of ~ 50 km/sec they obtained a modulating period of ~ 1000 seconds, consistent with their observations.

However, several explanations are possible for the observation of such quasi-periodic proton intensity variations. For example they may be due to i) an interaction with the magnetosphere, magnetosheath and/or bow shock regions, ii) source mechanism characteristics at or near the sun (this may not be the explanation for the event discussed by Bryant et al, (1965)). iii) A resonant interaction with hydromagnetic waves in the interplanetary medium or iv) the passage of a filamentary magnetic field having an inherent structural periodicity. As these phenomena effect the propagation of solar protons in the interplanetary medium it is of interest to learn which, if any, of the possible mechanisms dominate over an extended time period.

We present in this section preliminary results of a study of quasi-periodic variations in solar proton intensities as observed by the SPME 1-10 Mev channel onboard Explorer 34 (Williams et al, 1969). A more extensive report is now in preparation.

Variations with periods from tens of minutes to hours and which are observed to be both coupled to and independent of the local field and its fluctuations are often seen in the 1-10 Mev intensities. In order to treat these variations quantitatively, a time series analysis yielding a power spectrum of the fluctuations

has been performed on the 4 minute averaged 1-10 Mev data. The folding frequency is thus 0.125 cycles per minute ($\simeq 2.1\ (10)^{-3}$ Hz). Smooth trends in the data are removed by the application of a low pass filter. This is accomplished by subtracting a 100 point weighted running average from the data. The autocorrelation function and power spectrum are then obtained.

Figures 4 and 5 show data from time periods in which no noticeable intensity oscillations are present. Figure 4a shows 1-10 Mev proton intensity data for November 15-16, 1967 along with the ecliptic longitude ϕ and latitude θ, and magnitude $|B|$, of the local interplanetary magnetic field. The Explorer 34 magnetic field data have been generously made available to us by Drs. N. F. Ness and D. H. Fairfield.

The large field variations in θ are well outside the viewing cone (full angle = 60°) of the 1-10 Mev detector. The observation that the proton intensities in Figure 4a are independent of the field direction is thus indicative of a nearly isotropic flux.

The results of the time series analysis of the 1-10 Mev proton data in Figure 4a is shown in Figure 4b as a full logarithmic plot of the power spectrum. The frequency is given in cycles per minute and the power as (counts per sec)^2 per (cycle per minute). Multiplication by 21 converts the power to units of (directional flux)^2 per Hz.

Figure 4c shows a linear plot of the power spectrum given in Figure 4b along with a plot of the filter shape used in these analyses. The decrease in power at very low frequencies ($\lesssim 0.01$ CPM) is due to the low pass filter.

Figure 5 presents the data and power spectrum of the 1-10 Mev proton intensities from another period (October 31-November 1, 1967) in which no marked intensity variations were observed.

The results of the time series analysis for both the above periods show the power spectra to follow an f^{-1} to $f^{-1.5}$ power law. This is of interest as count rate data from a threshold detector which are random in time yield a flat (f^{0}) power spectrum, i.e., the individual data points are not correlated in time. The f^{-1} to $f^{-1.5}$ trend shown in Figures 4 and 5 indicates that the 1-10 Mev solar proton intensities are being ordered in the frequency domain by some as yet unknown mechanism.

Figures 6 and 7 present the 1-10 Mev intensities and power spectra for two periods in which quasi-periodic variations were observed. Figure 6a shows a small event on December 15, 1967 consisting of a sequence of oscillations with a period of a few tens of minutes. The power spectrum in Figure 6b shows a prominent peak at a period of 50 minutes and a possible secondary broader peak with a period of 20-25 minutes.

These oscillations do not appear to be controlled by the local magnetic field as there are no field variations in Figure 6a which are correlated with the proton variations. The power spectrum of the θ-component of the field also shows no prominent peaks during this time interval.

Figure 7 shows the 1-10 Mev proton intensity data and resultant power spectrum for the period November 2, 0452 hours through November 5, 0800 hours,

1967. The power spectrum in Figure 7b shows a peak at ~ .0125 CPM (period ~ 80 minutes). Visual inspection of Figure 7 shows that many of the proton intensity variations during this period are correlated with variations in the local magnetic field direction.

In summary, we have seen that the quiet time solar proton fluxes (1-10 Mev) appear to be ordered in the frequency domain by some as yet unknown mechanism. The power spectra for these cases show an f^{-1} to $f^{-1.5}$ trend over the frequency range 0.01 - 0.12 CPM ($1.7\ (10)^{-4}$ - $2(10)^{-3}$ Hz). We have also seen cases in which variations were present which displayed prominent peaks in the power spectra at 0.02 CPM (Figure 6) and 0.015 CPM (Figure 7). While a correlation with the local magnetic field was apparent in Figure 7, no such correlation could be made for the variations of December 16, 1967 in Figure 6. This latter event was thus not caused by the guiding of an anisotropic flux in and out of the detector collimating angle.

The gyroradius of a 1 Mev proton in a 5γ field is ~ $3\ (10)^4$ km ($2\ (10)^{-4}$ AU). A wave of this wavelength propagating in the interplanetary medium will have, depending on the direction of propagation, frequencies ranging to > 10^{-1} Hz in the proton's rest frame. Resonant interactions between these waves and the protons are possible as the proton gyrofrequency in a 5γ field is ~ $6\ (10)^{-2}$ Hz.

It is also possible that magnetospheric effects and/or source effects at the sun contribute to these variations. It is hoped that further studies will narrow down the choice of dominant mechanisms.

LOW ENERGY PROTON ENTRY INTO THE MAGNETOSPHERE

Indirect yet valuable information on the solar wind - magnetospheric interaction and the resulting magnetic field configuration can be obtained by studying the entry of low energy solar protons into the magnetosphere. Rapid and direct access of low energy solar protons to the polar cap and geomagnetic tail regions is predicted if a large fraction of the earth's high latitude field lines directly connect to interplanetary field lines, as in an "open" magnetospheric configuration (Dungey, 1961). In the absence of significant interconnection diffusive effects will govern the entry of such protons into the magnetosphere. Consequently, time delays should be observed between the arrival of protons outside of and within the magnetosphere. Such effects in an extended geomagnetic tail configuration (Piddington, 1960; Dessler, 1964; Axford et al, 1965; Dessler and Juday, 1965) having no significant interconnection have been considered by Michel (1965) in discussing cosmic-ray cutoffs and by Michel and Dessler (1965) in discussing polar cap absorption in homogeneities. They have obtained tail length and delay time estimates of ≥ 1 AU and a few hours respectively. We shall see that these early estimates are not in quantitative agreement with available solar proton observations.

Williams and Bostrom (1967) have argued that variations in the mode of entry of low energy solar protons into the magnetosphere are expected since this entry is controlled by the existing magnetospheric configuration which in turn depends on the boundary conditions imposed by the interplanetary medium. They

have used this argument to explain large observed pass to pass fluctuations in low energy solar proton polar cap averages during the February 5, 1965 event which were not present in the interplanetary regions.

Krimigis et al, (1967) have reported that for the July 7, 1966 event low energy solar protons had access to the earth's polar caps within 30 minutes after their arrival in the near-earth interplanetary region. While not conclusively supporting either an "open" or a "closed" magnetosphere, these data did show quantitative disagreement with earlier tail length - delay time estimates (Michel and Dessler, 1965).

Polar cap proton intensity profiles showing enhanced fluxes in the auroral regions have been reported by Blake et al, (1968) and presented by Bostrom et al, (1967) and Zmuda et al, (1967). Such profiles do not support field line interconnection (which requires a uniform polar cap intensity profile within minutes of the arrival of solar protons) and are in qualitative agreement with diffusive entry.

A recent study (Williams and Bostrom, 1969) has presented evidence indicating that a diffusion process controlled the entry of protons into the magnetosphere on May 26, 1967. Proton intensities in the interplanetary medium were obtained from the 1-10 Mev SPME channel onboard Explorer 34 and 1.2 - 8.5 Mev proton intensities over the northern polar cap were obtained from satellite 1963 38C. We shall summarize these results using Figures 8, 9, and 10 (from Williams and Bostrom, 1969).

Figure 8 shows the time period studied and presents interplanetary 1-10 Mev proton intensities, polar cap 1.2 - 8.5 Mev proton intensities, Dst, and a summation of the interplanetary field direction (D. H. Fairfield, K. W. Behannon and N. F. Ness, personal communications). The absolute unnormalized fluxes shown in Figure 8 point out that while general similarities exist between these two regions, significant differences in the respective time histories do occur. In particular it is seen that, a) the ratio of polar cap to interplanetary fluxes varies by a factor of ~ 3 during the period shown, and b) the significant decrease in the interplanetary fluxes occurring at ~ 1120 hours (Figure 8) is not observed over the polar cap. These features do not support the existence at these times of a radily accessible polar cap region as in an open magnetospheric configuration. They are qualitatively consistent with low energy proton access to the polar cap being controlled by a diffusion process.

Figure 9 shows the time sequence of five passes (1-5 in Figure 8) obtained during a period in which a slight increase occurred in the interplanetary intensities. Here is clearly seen a time history of polar cap protons which progresses from pass 1 where the intensities tend to increase toward the polar cap, to passes 2, 3, and 4 which show a profile peaked near the auroral regions and having a minimum at the highest latitudes, to pass 5 which shows a distribution much more uniform over all latitudes sampled.

The general features of these polar cap observations can be explained by the magnetotail configuration shown in Figure 10 a, b. A Figure-8 tail current

system defines two approximately cylindrical surfaces which when coupled with the rotation of the earth contain the field lines connecting to the low latitude edge of the northern and southern polar caps (Dessler and Juday, 1965; Axford et al., 1965). Diffusion into the tail region should produce polar cap profiles which are initially peaked near the auroral regions and which gradually fill in the high latitude polar cap region in much the same manner as shown in Figure 9.

A rough estimate of the magnitude of the diffusion coefficient may be obtained by considering diffusion into a long cylinder of radius a, (Figure 10a), which has an internal density of zero and in which diffusion is purely radial. Figure 10c presents the solution to this problem by showing the radial density profile for several different times following the application of an external and steady source of strength n_o [Crank, 1957). The similarity of the radial profiles in Figure 10c to the polar cap profiles of Figure 9 is readily apparent. (Note that $r\ a = 0$ corresponds roughly to $\Lambda = \pi/2$ and $r\ a = 1$ to the nightside auroral oval.) The ratio of polar cap to auroral oval intensities will be assumed to yield $n\ n_o$, the ratio of internal to external densities, at $r\ a = 0$. Figure 10c thus yields the appropriate value of $Dt\ a^2$ from which D can be obtained.

Pass 4 in Figure 9 gives a polar cap to auroral region ratio of $n\ n_o \approx 0.4$ yielding (from Figure 10c) a value of $Dt\ a^2 \sim 0.15$. Due to the gap in the Explorer 34 intensities, the appropriate value of t can only be estimated from Figure 2 as $t \approx$ 1.5-5 hours. Using $a = 20\ R_E$ gives $D = 1.4\ (10)^{15} - 4.0\ (10)^{15}$ cm^2/sec.

The value of D obtained in the above analysis is considered a first approximation to the value of the radial component $D_{r,r}$, of the diffusion tensor. The relative magnitude of the component along the field line, $D_{z,z}$, cannot be obtained in this analysis and depends on assumptions used in estimating pitch angle scattering effects.

As the above analysis gives no information about $D_{z,z}$, it can give no accurate estimate on the "length" of the tail, i.e., the distance to the region where particles begin to be diffused into the magnetosphere. A crude upper limit value on this length is obtained by assuming rectilinear motion of the protons down the tail to the auroral regions where they first appear. The timing and structural response of passes 8 and 10 in Figure 8 to the two small flux increases observed in the interplanetary data yield an upper limit for the tail length L, of (Williams and Bostrom, 1969)

$$L \leq (420 - 2400)\, R_E$$

Note that the region of entry for low energy solar protons into the tail may be closer to the earth, depending on the magnitude of $D_{z,z}$.

It was further noted by Williams and Bostrom (1969) that the rapid access of low energy protons to the entire Figure-8 current pattern and resulting diffusion into the cylinders (arrows in Figure 10b) can qualitatively account for the appearance of peak proton intensities near the auroral regions and the latitude spread ($\sim 10°$) of this peak. However, such a configuration is unable to quantitatively account for observed low energy proton cutoffs, particularly on the dayside hemisphere.

The ready access of low energy solar protons to 6.6 R_E (Lanzerotti, 1968) may be directly related to their appearance in the neutral sheet. The diffusion effects discussed by Lanzerotti (1968) may in this case be related to diffusion through the "cusp" region and not to radial diffusion through the tail.

Delayed access ($\geq$ 15 minutes) of low energy solar protons to the geomagnetic tail is often directly observed (Kane et al, 1968; Montgomery and Singer, 1969). In addition, Montgomery and Singer (1969) report that anisotropic proton fluxes observed in the interplanetary medium become isotropic when observed in the magnetotail. These authors also report the lack of a strong energy dependence in the observed delay times and the lack, at times, of any significant broading of intensity structure when observed within the magnetotail. Montgomery and Singer (1969) have interpreted these results as indicative of a mixed mode of proton entry where both diffusive effects and direct entry are simultaneously operative.

Observed enhancements of 1.2-2.2 Mev solar proton intensitive at high latitudes ($\Lambda \sim 80°$) have been associated with the high latitude topology of the magnetopause (Williams and Bostrom, 1967; Williams et al, 1968). Such enhancements may be the effect of a high latitude neutral line on the magnetopause or an indication of the first geomagnetic field line to interconnect with the interplanetary field.

Figure 11 shows a polar cap latitude profile in which the proton intensity increases by a factor of ~ 3 at $\Lambda \sim 78°$. The existence of a day-night assymetry

can also be seen. The interplanetary proton intensities are seen to be steady throughout the pass. The interplanetary field at the time was strongly ($\lambda_{GSE} \simeq -40°$) southward and had been so for the preceding several days (D. H. Fairfield, personal communication). It is thus possible that the enhancement in Figure 11 may indicate the latitude of the first interconnecting geomagnetic field line. However, Williams and Bostrom (1969) point out that a southward interplanetary magnetic field may not be a sufficient condition for direct proton access to the magnetosphere since diffusive effects are seen under such conditions.

Simultaneous observations of solar electrons within and outside of the magnetopause have not yet been reported. However, Lin (1968) and Anderson (1969) have used lunar shadowing effects on ≥ 40 kev electron angular distributions in the magnetotail to argue for the direct entry of solar electrons deep within the tail regions. Vampola (1969) has reported isotropic electron fluxes which are flat and featureless over the polar caps and which do not uniquely favor either diffusion or direct access. We note that electron access to the magnetosphere may be quite different from proton access due to the large difference in gyroradii.

For protons, the mode of access seems governed by the magnetospheric configuration existing at the time (Williams and Bostrom, 1967). Therefore strong variations in the manner in which low energy protons enter the magnetosphere are to be expected. Diffusive effects, direct access, or various intermediate cases may be observed at any particular time. In addition, diffusive effects are operative on time scales and within tail length estimates much shorter than previously estimated.

ACKNOWLEDGMENTS

I gratefully acknowledge and thank my colleagues, Drs. J. F. Arens, C. O. Bostrom, and Mr. M. L. Dwarkin, for allowing me to discuss some of our preliminary results on interplanetary proton intensity oscillations prior to publication. I also thank Drs. L. F. Burlaga, S. M. Krimigis, and E. C. Roelof for their helpful discussions and assistance. Finally I thank Drs. D. H. Fairfield and N. F. Ness and Mr. K. W. Behannon for the use of magnetic field data from Explorers 33 and 34.

REFERENCES

Anderson, K. A., "Electrons and Protons in Long-Lived Streams of Energetic Solar Particles", Solar Physics, 6, 111-132, 1969.

Anderson, K. A., "Observation of Interplanetary Field Lines in the Magnetotail", Preprint, Space Sciences Laboratory, University of California Berkeley, March 3, 1969.

Axford, W. I., "Anisotropic Diffusion of Solar Cosmic Rays" Planetary Space Sci., 13, 1301-1309, 1965.

Axford, W. I., H. E. Petschek, and G. L. Siscoe, "The Tail of the Magnetosphere", J. Geophys. Res., 70, 1231-1236, 1965.

Bartley, W. C., R. P. Bukata, K. G. McCracken, and U. R. Rao, "Anisotropic Cosmic Radiation Fluxes of Solar Origin", J. Geophys. Res., 71, 3297-3304, 1966.

Blake, J. B., G. A. Paulikas, and S. C. Freden, "Latitude Intensity Structure and Pitch Angle Distributions of Low Energy Solar Cosmic Rays at Low Altitude", J. Geophys. Res., 73, 4927-4934, 1968.

Bostrom, C. O., J. W. Kohl, and A. J. Zmuda, "The Solar Proton Events of August 29 and September 2, 1966" (abstract) Trans. Am. Geophys. Union, 48, 178, 1967.

Bryant, D. A., T. L. Kline, U. D. Desai and F. B. McDonald, "Explorer 12 Observations of Solar Cosmic Rays and Energetic Storm Particles Following the Solar Flare of September 28, 1961," J. Geophys. Res., 67, 4983-5000, 1962.

Bryant, D. A., T. L. Cline, U. D. Desai, and F. B. McDonald, "Studies of Solar Protons with Explorers XII and XIV", Astrophys. J., 141, 478-499, 1965.

Burlaga, L. F., "Anisotropic Diffusion of Solar Cosmic Rays", J. Geophys. Res., 72, 4449-4466, 1967.

Crank, J., "The Mathematics of Diffusion", Oxford University Press, 1957.

Dessler, A. J., "Length of the Geomagnetic Tail", J. Geophys. Res., 69, 3913-3918, 1964.

Dessler, A. J. and R. D. Juday, "Configuration of Auroral Radiation in Space", Planet. Space Sci., 13, 63-72, 1965.

Dolginov, A. Z., and I. M. Toptygin, "Diffusion of Cosmic Particles in the Interplanetary Medium", Geomag. and Aeron., 7, 785-790, 1967.

Dungey, J. W., "Interplanetary Magnetic Field and the Auroral Zones", Phys. Rev. Let., 6, 47-48, 1961.

Fan, C. Y., J. E. Lamport, J. A. Simpson, and D. R. Smith, "Anistrophy and Fluctuations of Solar Proton Fluxes of Energies 0.6-100 Mev Measured on Pioneer 6 Space Probe", J. Geophys. Res., 71, 3289-3296, 1966.

Fan, C. Y., M. Pick, R. Pyle, J. A. Simpson, and D. R. Smith, "Protons Associated with Centers of Solar Activity and Their Propagation in the Interplanetary Magnetic Field Regions Co-rotating with the Sun", J. Geophys. Res., 73, 1555-1582, 1968.

Fichtel, C. E., and F. B. McDonald, "Energetic Particles from the Sun", Annual Rev. of Astronomy and Astrophys., 5, 351-398, 1967.

Hofmann, D. J., and J. R. Winckler, "Simultaneous Balloon Observations at Fort Churchill and Minneapolis during the Solar Cosmic Ray Events of July 1961", J. Geophys. Res., 68, 2067-2098, 1963.

Jokipii, J. R., "Cosmic Ray Propagation 1, Charged Particles in a Random Magnetic Field", Astrophys. J., 146, 480-487, 1966.

Kane, S. R., J. R. Winckler, and D. J. Hoffman, "Observations of Screening of Solar Cosmic Rays by the Outer Magnetosphere", Planet. Space Sci., 16, 1381-1404, 1968.

Kavanaugh, L. D., A. W. Schardt, and E. C. Roelof, "Solar Wind and Solar Energetic Particles: Properties and Interactions", Preprint March, 1969, to be published in Reviews of Geophysics.

Krimigis, S. M., "Interplanetary Diffusion Model for the Time Behavior of Intensity in a Solar Cosmic Ray Event", J. Geophys. Res., 70, 2943-2960, 1965.

Krimigis, S. M., and J. A. Van Allen, "Observation of ~500 kev Protons in Interplanetary Space with Mariner 4", Phys. Rev. Let., 16, 419-423, 1966.

Krimigis, S. M., J. A. Van Allen, and T. P. Armstrong, "Simultaneous Observations of Solar Protons Inside and Outside the Magnetosphere", Phys. Rev. Letters, 18, 1204-1207, 1967.

Lanzerotti, L. J., "Penetration of Solar Protons and Alphas to the Geomagnetic Equator", Phys. Rev. Letters, 21, 929-933, 1967.

Lin, R. P., S. W. Kahler, and E. C. Roelof, "Solar Flare Injection and Propagation of Low Energy Protons and Electrons in the Event of 7-9 July 1966", Solar Physics, 4, 338-360, 1968.

Lin, R. P., and K. A. Anderson, "Electrons ≥ 40 kev and Protons ≥ 500 kev of Solar Origin", Solar Physics, 1, 446-464, 1967.

Lin, R. P., "Observations of Lunar Shadowing of Energetic Particles", J. Geophys. Res., 73, 3066-3071, 1968.

Lüst, R., and J. A. Simpson, "Initial Stages in the Propagation of Cosmic Rays Produced by Solar Flares", Phys. Rev., 108, 1563-1576, 1957.

McCracken, K. G., "The Cosmic Ray Flare Effect 2. The Flare Effects of May 4, November 12, and November 15, 1960", J. Geophys. Res., 67, 435-446, 1962.

McCracken, K. G., and N. F. Ness, "The Collimation of Cosmic Rays by the Interplanetary Magnetic Field", J. Geophys. Res., 71, 3315-3318, 1966.

McCracken, K. G., U. R. Rao, and R. P. Bukata, "Cosmic Ray Propagation Processes 1, A Study of the Cosmic Ray Flare Effect", J. Geophys. Res., 72, 4293-4324, 1967.

McCracken, K. G., U. R. Rao, and N. F. Ness, "Interrelationship of Cosmic Ray Anisotropies and the Interplanetary Magnetic Field", J. Geophys. Res., 73, 4159-4166, 1968.

Meyer, P., E. N. Parker, and J. A. Simpson, "Solar Cosmic Rays of February 1956 and their Propagation through Interplanetary Space", Phys. Rev., 104, 768-783, 1956.

Michel, F. C., "Effect of Magnetospheric Tail on Cosmic-Ray Cut-Offs", Planet. Space Sci., 13, 753-760, 1965.

Michel, F. C. and A. J. Dessler, "Physical Significance of Inhomogeneities in Polar Cap Absorption Events", J. Geophys. Res., 70, 4305-4311, 1965.

Montgomery, M. D. and S. Singer, "Penetration of Solar Energetic Protons Into the Magnetotail", J. Geophys. Res., 74, 2869-2880, 1969.

Morrison, P., "Solar Origin of Cosmic-Ray Time Variations", Phys. Rev., 101, 1397-1404, 1956.

Parker, E. N., "Modulation of Primary Cosmic-Ray Intensity", Phys. Rev., 103, 1518-1533, 1956.

Parker, E. N., "Dynamics of the Interplanetary Gas and Magnetic Fields", Astrophys. J., 128, 664-676, 1958.

Parker, E. N., Interplanetary Dynamical Processes, John Wiley and Sons, New York, 1963.

Piddington, J. H., "Geomagnetic Storm Theory", J. Geophys. Res., 65, 93-105, 1960.

Reid, G. C., "A Diffusive Model for the Initial Phase of a Solar Proton Event", J. Geophys. Res., 69, 2659-2667, 1964.

Roelof, E. C., "Statistical Theory of Charged Particle Transport in Disordered Magnetic Field", Ph.D. Dissertation, University of California Berkeley, Dec. 1966.

Solar Geophysical Bulletin, IER-FB-282, Feb. 1968 and monthly thereafter.

Webber, W. R., "A Review of Solar Cosmic Ray Events", AAS-NASA Symposium of the Physics of Solar Flares, NASA SP-50, edited by W. N. Hess, 215-254, 1963.

Williams, D. J. and C. O. Bostrom, "The February 5, 1965 Solar Proton Event. 2. Low Energy Solar Protons and Their Relation to the Magnetosphere", J. Geophys. Res., 72, 4497-4506, 1967.

Williams, D. J., J. F. Arens, J. W. Kohl, and C. O. Bostrom, "Observations of Low Energy Protons During the May 28, 1967 Event", (abstract) Midwest Cosmic Ray Conference, March, 1968.

Williams, D. J., J. F. Arens, C. O. Bostrom, and M. L. Dwarkin, "Oscillations of 1-10 Mev Proton Intensities in Interplanetary Space", (abstract), Trans. Am. Geophys. Union, 50, 300, 1969.

Williams D. J., and C. O. Bostrom, "Proton Entry into the Magnetosphere on May 26, 1967", J. Geophys. Res., 74, 3019-3026, 1969.

Vampola, A. L., "Energetic Electrons at Latitudes above the Outer-Zone Cutoff", J. Geophys. Res., 74, 1254-1269, 1969.

Zmuda, A. J., J. W. Kohl, and C. O. Bostrom, "The Solar Proton Event of September 2, 1966: Day and Night Latitude Profiles", (abstract) Trans. Am. Geophys. Union, 48, 178, 1967.

FIGURE CAPTIONS

Figure 1. Hourly averages of solar proton intensities for the period May 24 - May 31, 1967. Data from the Solar Proton Monitoring Experiment onboard the Explorer 34 satellite. Satellite position shown below proton intensities as a plot of the radial distance to the satellite (apogee 34.5 R_E) and as a projection of the orbit into the ecliptic plane. The high intensity points near perigee are due to the earth's radiation belts. Note that the ≥10 Mev channel is significantly more sensitive to the trapping regions than the other detecting channels. To convert to flux values when solar protons are present, the appropriate geometric factors to use for the ≥60 Mev, ≥30 Mev, ≥10 Mev, and 1-10 Mev channels are 2π cm^{2}ster, 2πcm^{2}ster, 0.79 cm^{2}ster, and 1.7 cm^{2}ster respectively.

Figure 2. Same as Figure 1 for June 1967.

Figure 3. Same as Figure 1 for the period August 9-13, 1967. Note the very soft spectrum for this event.

Figure 4. 1-10 Mev solar proton intensities and power spectrum for the relatively quiet period November 15-16, 1967. Observations obtained in the interplanetary medium, and 70° W of the earth-sun line.

a) 1-10 proton intensities, solar ecliptic latitude θ, longitude ϕ, and magnitude $|B|$ of local interplanetary magnetic field.

b) power spectrum of proton intensity data with reference f^{-1} and $f^{-1.5}$ curves. Power given as (counts/sec)^2 per cycle per minute.

c) linear plot of power spectrum shown in b) along with plot of low pass filter shape.

Figure 5. Same as Figure 4 for the period October 31, 0716 hours through November 1, 0712 hours, 1967. Data from interplanetary regions, 55°W of earth-sun line. a) solar proton intensities and interplanetary magnetic field, b) power spectrum of proton data.

Figure 6. Same as Figure 5 for the active period of 0000 hours through 1512 hours December 16, 1967. Data from interplanetary regions, 100°W of earth-sun line. Note the very prominent peak in the proton power spectrum at a frequency of 0.02 CPM ($\sim 3.3\ (10)^{-4}$ Hz).

Figure 7. Same as Figure 5 for the period of November 2, 0452 hours through November 5, 0800 hours, 1967. Data from interplanetary regions, 56°W of earth-sun line. Note significant peak in power spectrum of proton intensities at 0.0125 CPM ($2.1\ (10)^{-4}$ Hz).

Figure 8. Time history of 1-10 Mev protons observed at high altitudes ($\geq 28.2\ R_E$) and 1.2-8.5 Mev protons observed at 1100 km over the northern polar cap. The high altitude data are plotted as 15-minute averages and the polar cap data are averages for invariant latitudes >70°. The data shown are absolute an unnormalized fluxes. Orientation of the interplanetary magnetic field with respect to the ecliptic plane is indicated. From Williams and Bostrom, (1969).

Figure 9. High latitude proton intensity profiles from 1963 38C for passes 1-5 from Figure 8. Simultaneous Explorer 34 data shown were available. Flux values are unnormalized. Explorer 34 altitude ~32 R_E. Error bars show statistical uncertainties. From Williams and Bostrom, (1969).

Figure 10. (a) Sketch of magnetospheric configuration: (b) The current pattern in the tail region (after Axford et al., 1965, and Dessler and Juday, 1965). Heavy arrows indicate current flow and light arrows indicate proton diffusion: (c) Resulting radial diffusion pattern in a long cylinder of radius a, with initial internal density of zero, following application of an external, n_o. The internal density distribution, n/n_o, is shown as a function of r/a for various values of Dt/a^2 where D - diffusion coefficient and t - time following application of the external density, n_o. From (a) it can be seen that these radial profiles transform to polar cap latitude profiles in the following approximate way: r/a = 0 corresponds to $\Lambda = \pi/2$ and r/a = 1 corresponds to the auroral region. From Williams and Bostrom, (1969).

Figure 11. Plot of solar proton intensities obtained from satellite 1963 38C over northern polar cap from 1501-1511 hours on May 30, 1967. Simultaneous interplanetary solar protons intensities obtained from satellite Explorer 34 are also shown. Interplanetary field at this time was southward at $\theta \geq -40°$ (D. H. Fairfield, personal

communication). Of interest is the large step in polar cap intensities occurring at an invariant latitude $\Lambda \sim 78°$ at 0750 hours local time.

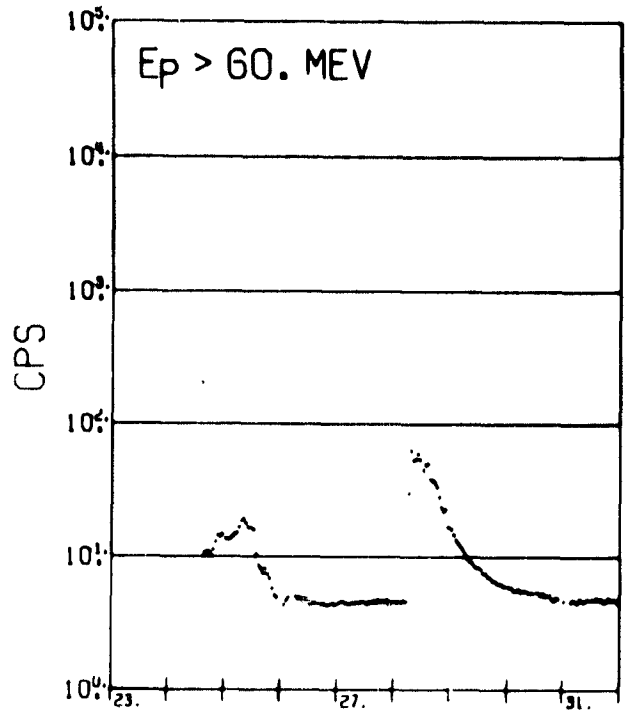

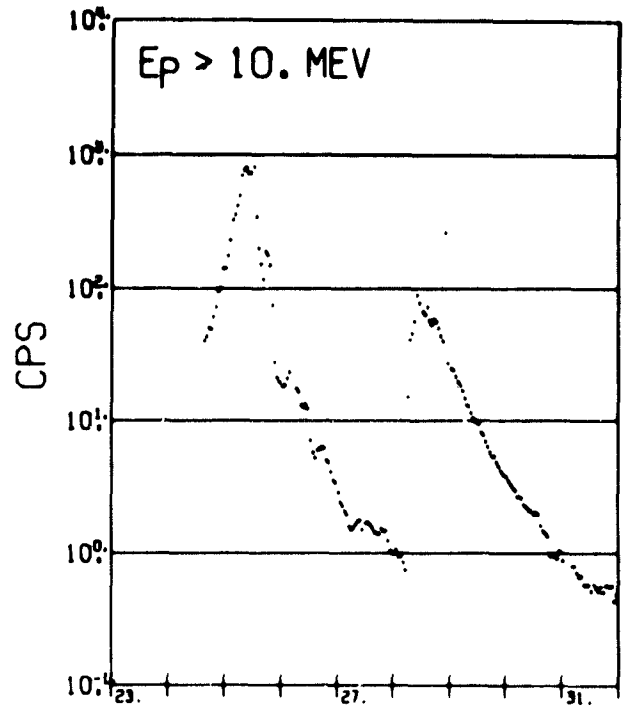

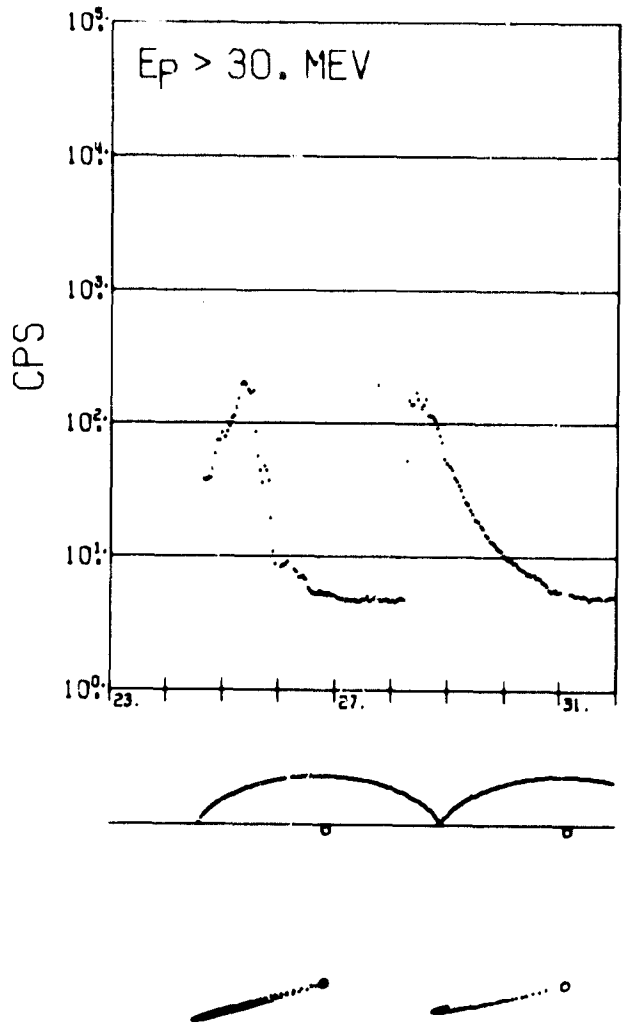

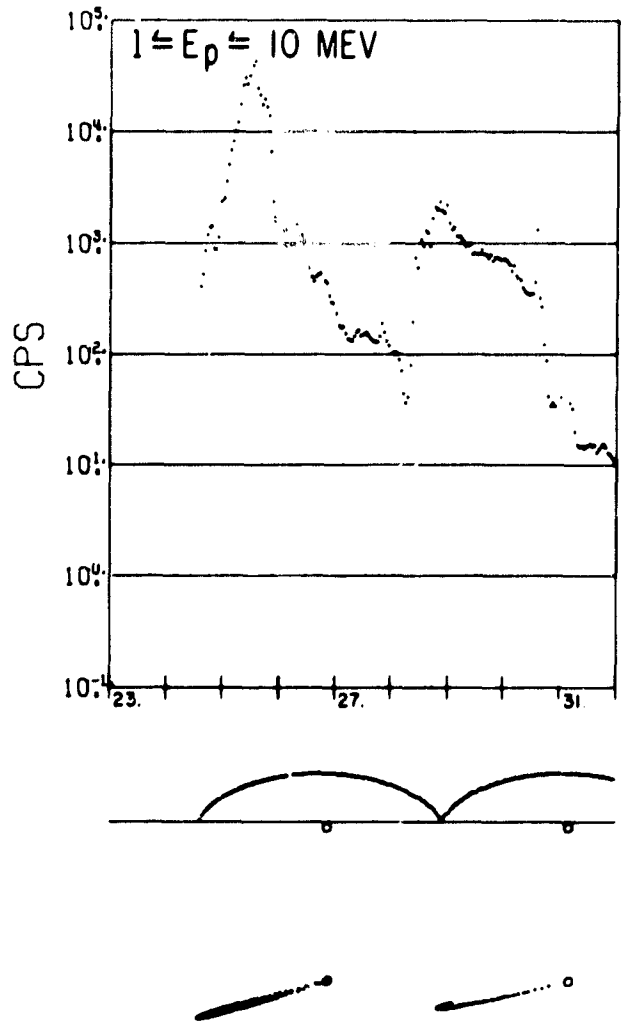

MAY 1967

FIGURE 1

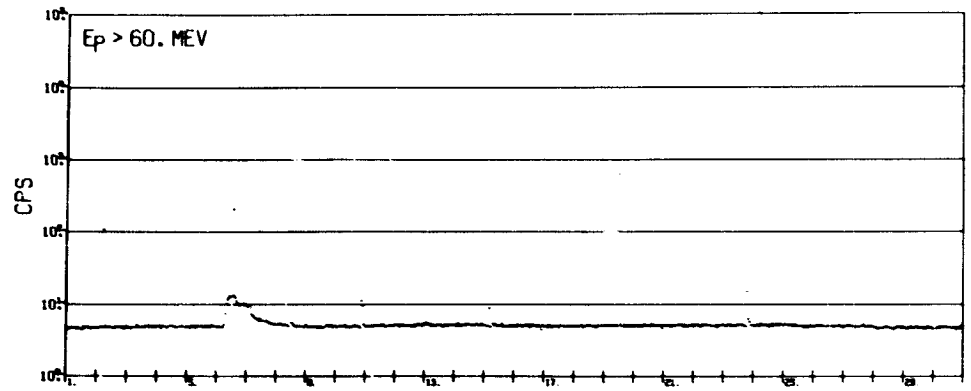

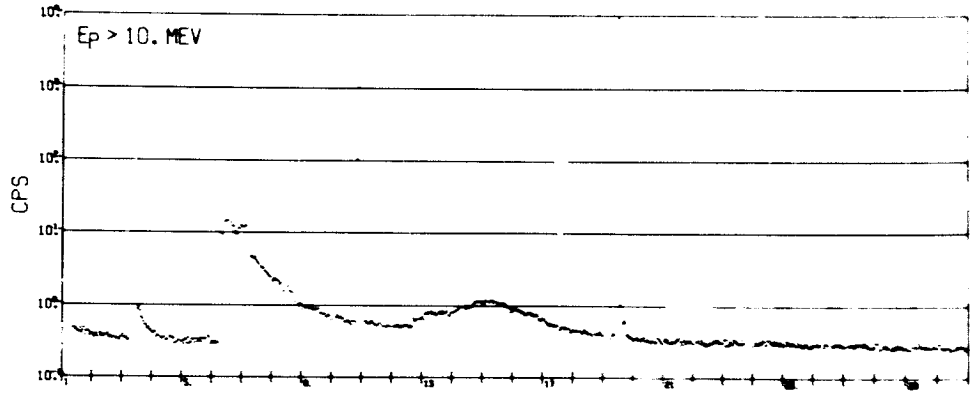

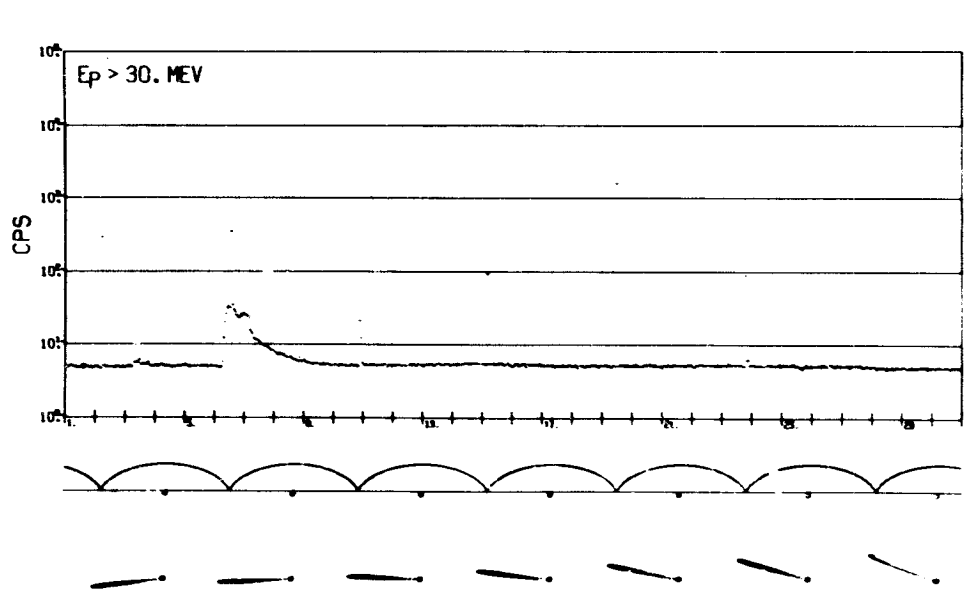

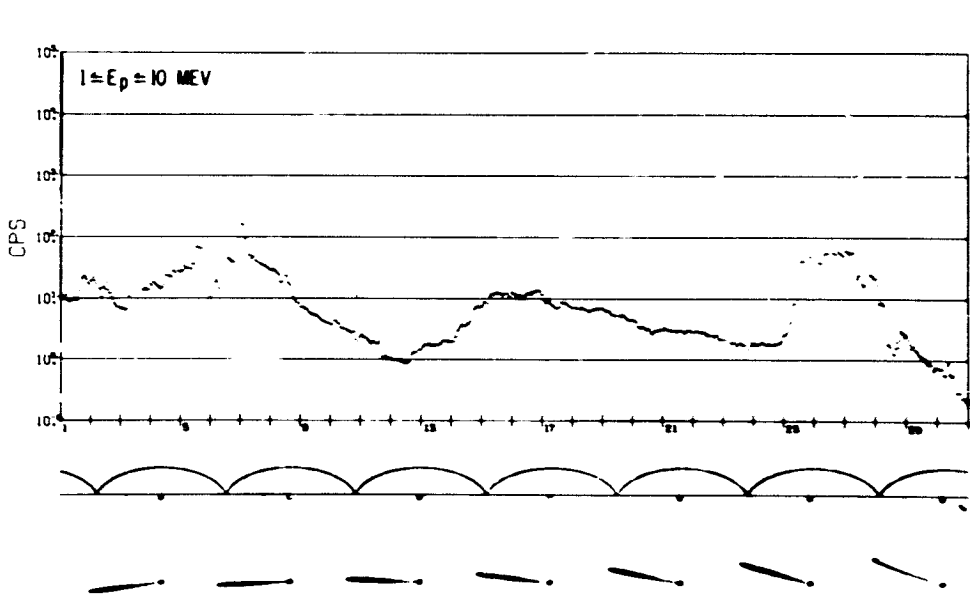

JUNE 1967

FIGURE 2

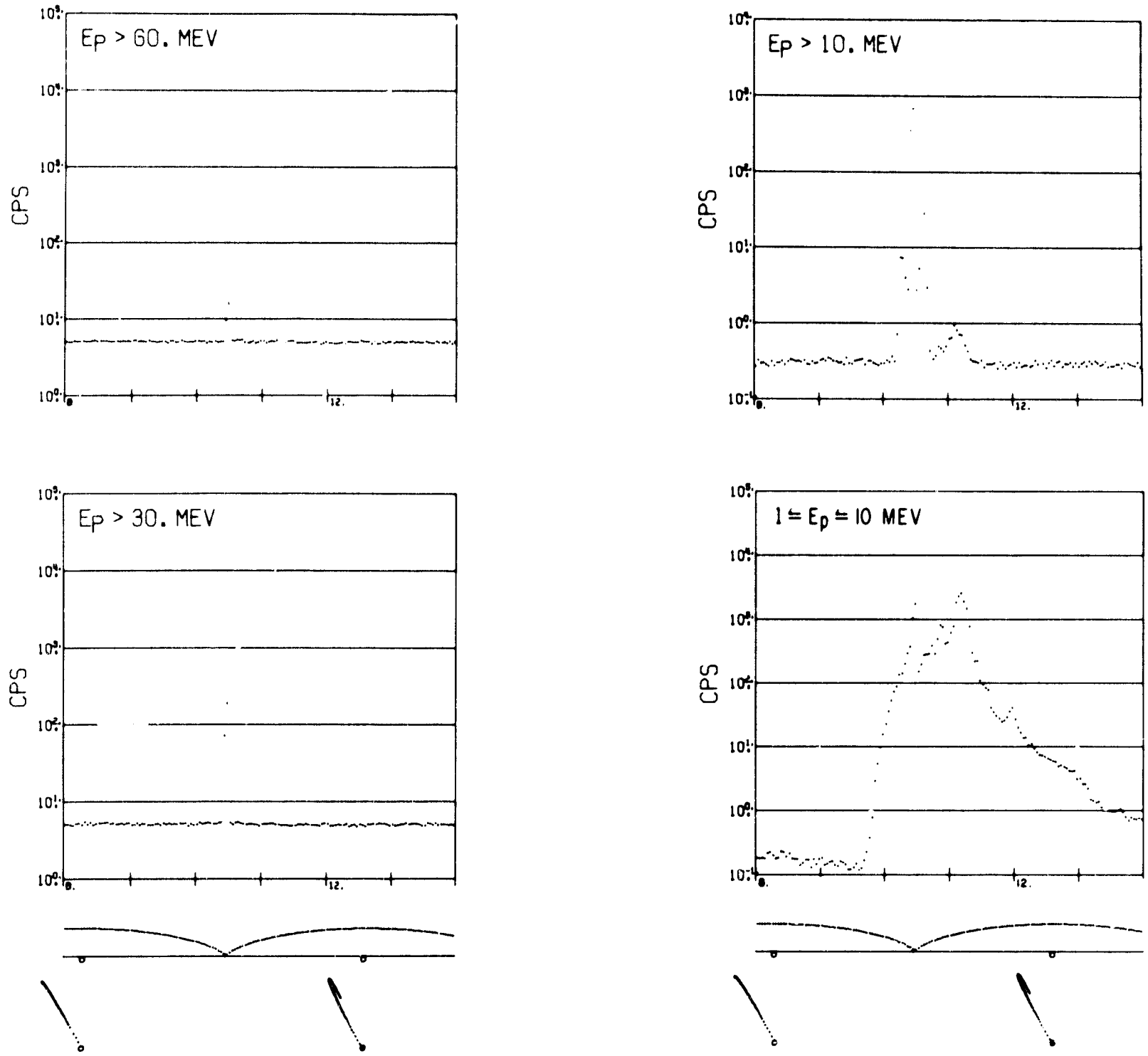

AUGUST 1967

FIGURE 3

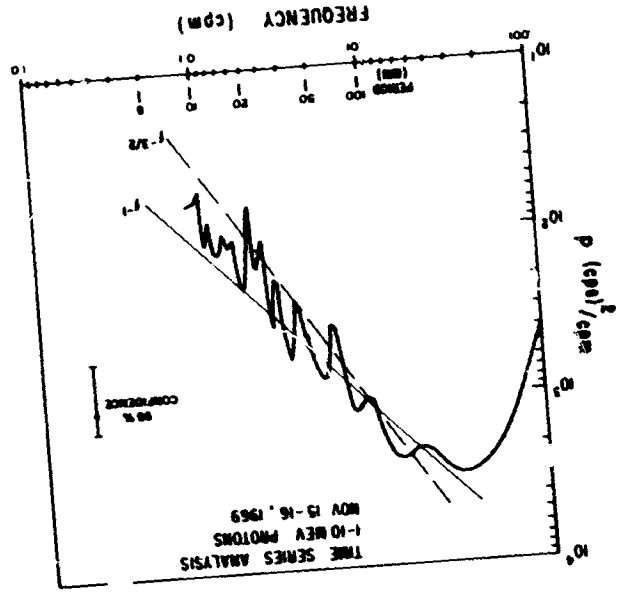
FREQUENCY (cpm)
TIME SERIES ANALYSIS
1-10 MEV PROTONS
NOV 15-16, 1969

(b)

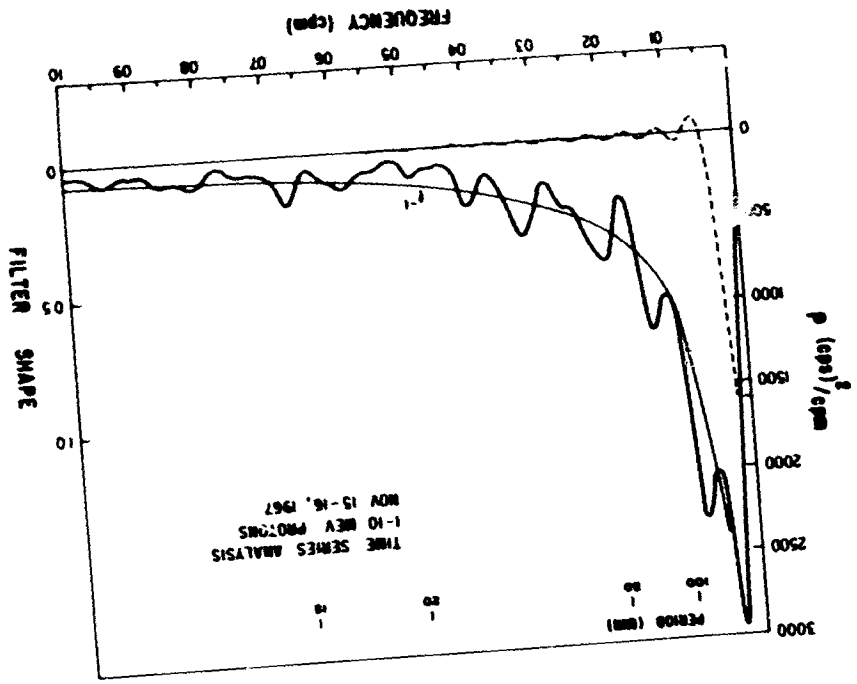
FREQUENCY (cpm)
FILTER SHAPE
TIME SERIES ANALYSIS
1-10 MEV PROTONS
NOV 15-16, 1967

(c)

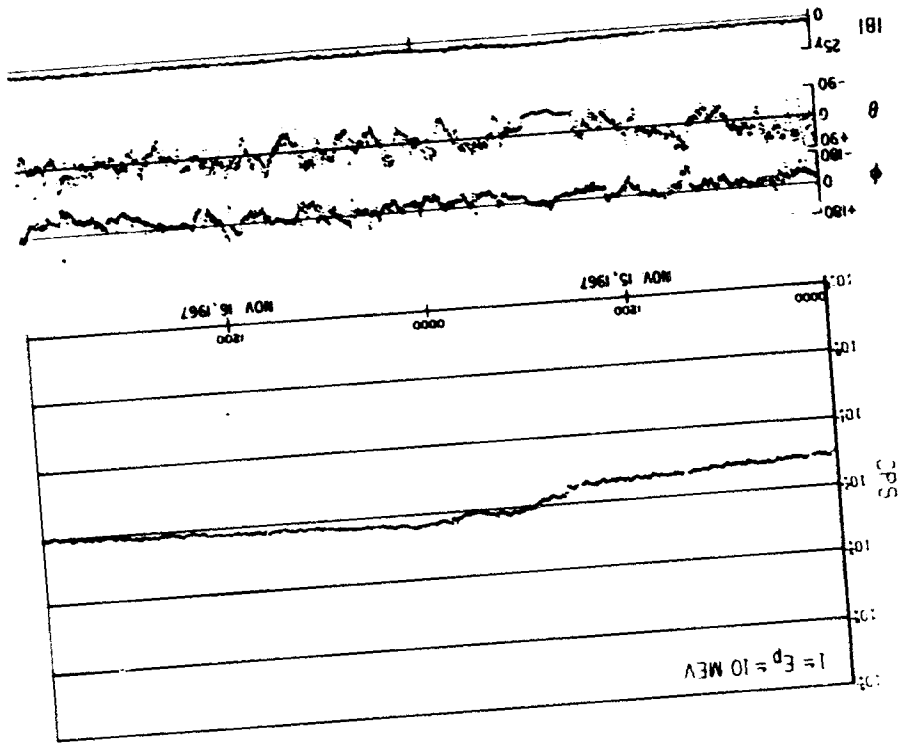
B
θ
φ
NOV 15, 1967
NOV 16, 1967
I = Ep = 10 MEV

(d)

(a)

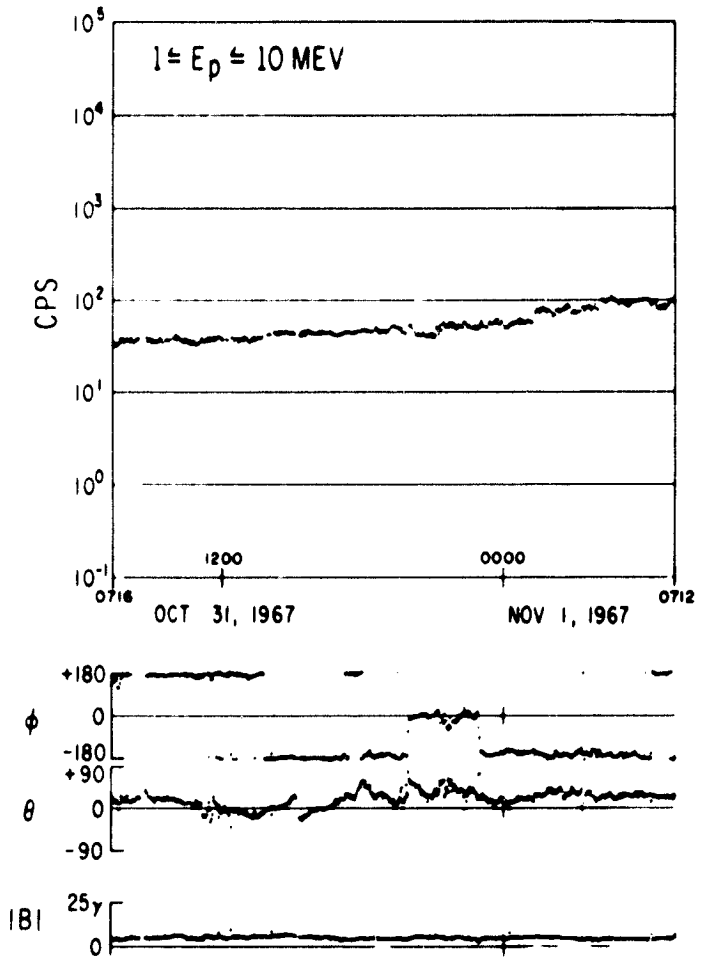
1 ≤ Ep ≤ 10 MEV
CPS
10^5
10^4
10^3
10^2
10^1
10^0
10^-1
1200
0000
0716
0712
OCT 31, 1967
NOV 1, 1967
+180
0
-180
φ
+90
0
-90
θ
|B|
25γ
0

(b)

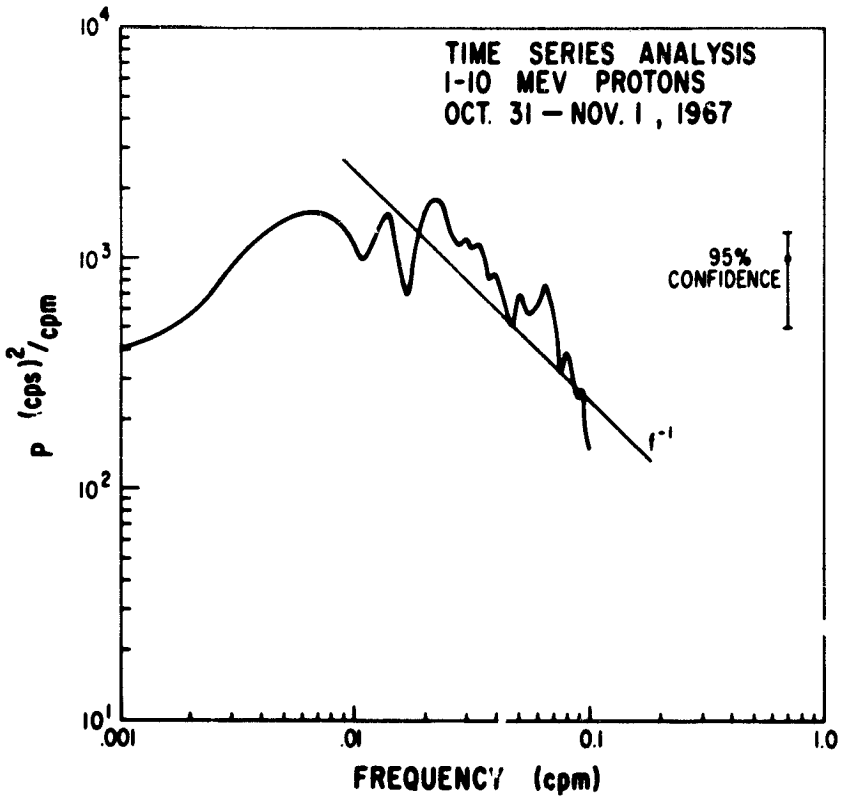
TIME SERIES ANALYSIS
1-10 MEV PROTONS
OCT. 31 — NOV. 1, 1967
95% CONFIDENCE
f^-1
P (cps)^2/cpm
10^4
10^3
10^2
10^1
.001
.01
0.1
1.0
FREQUENCY (cpm)

FIGURE 5

(a)

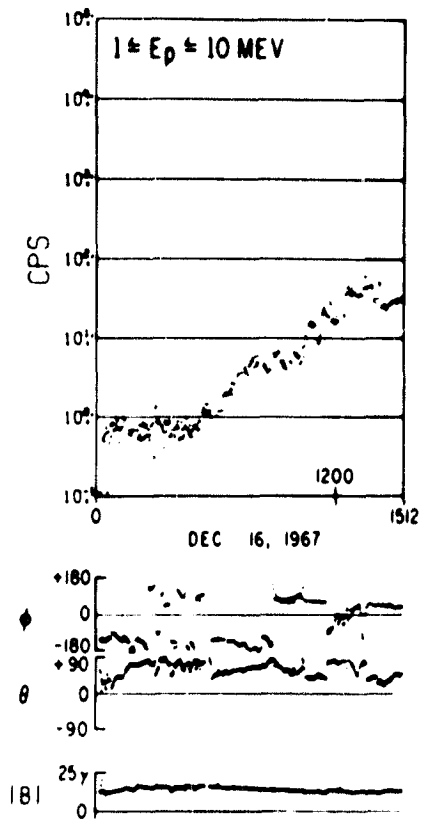
1 ≤ Ep ≤ 10 MEV
CPS
1200
0
1512
DEC 16, 1967
+180
0
-180
+90
0
-90
φ
θ
|B|
25γ
0

(b)

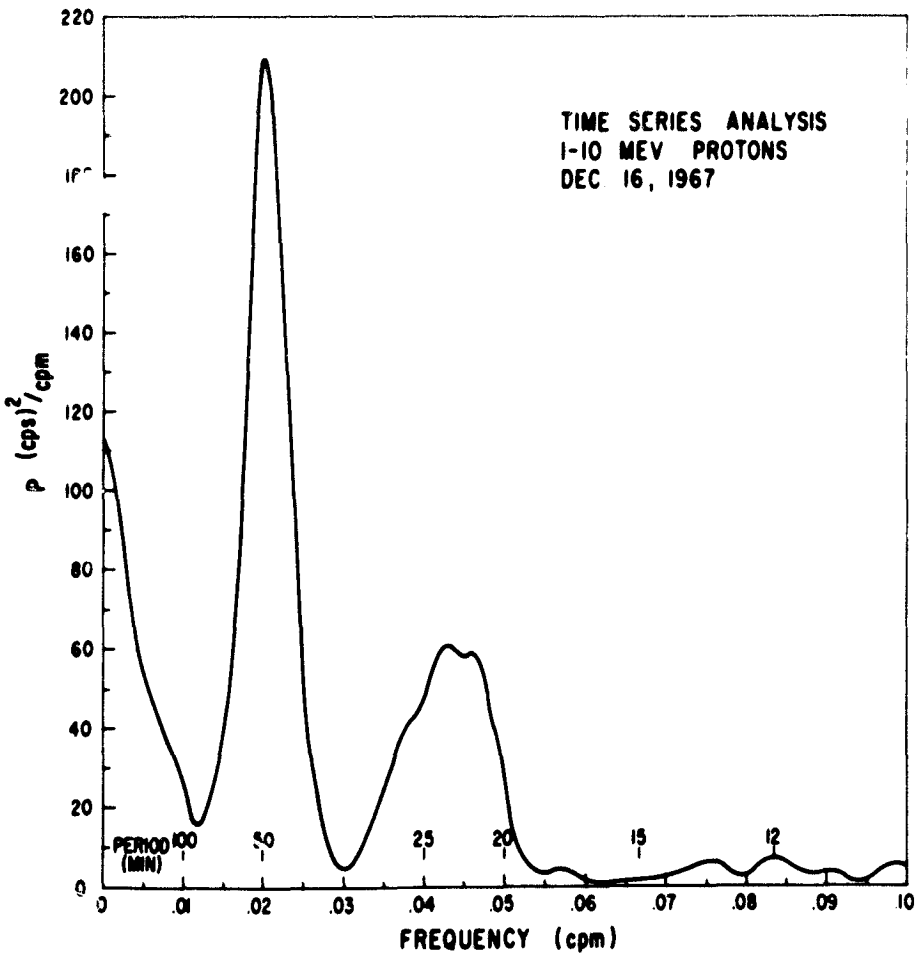
TIME SERIES ANALYSIS
I-10 MEV PROTONS
DEC 16, 1967
P (cps)²/cpm
PERIOD (MIN)
100
50
25
20
15
12
FREQUENCY (cpm)

FIGURE 6

(a)

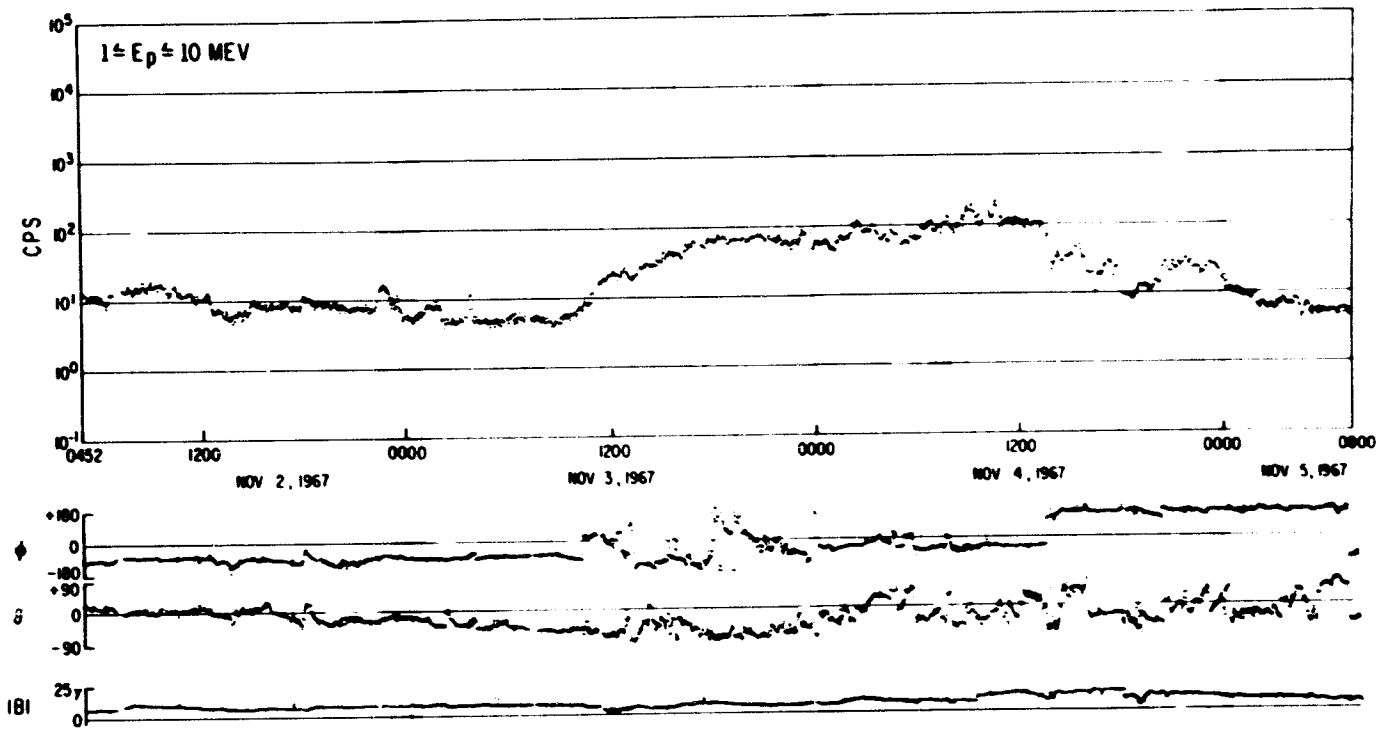
1 ≤ Ep ≤ 10 MEV
CPS
10^5
10^4
10^3
10^2
10^1
10^0
10^-1
0452
1200
0000
1200
0000
1200
0000
0800
NOV 2, 1967
NOV 3, 1967
NOV 4, 1967
NOV 5, 1967
+180
0
-180
φ
+90
0
-90
δ
25γ
0
181

FIGURE 7

(b)

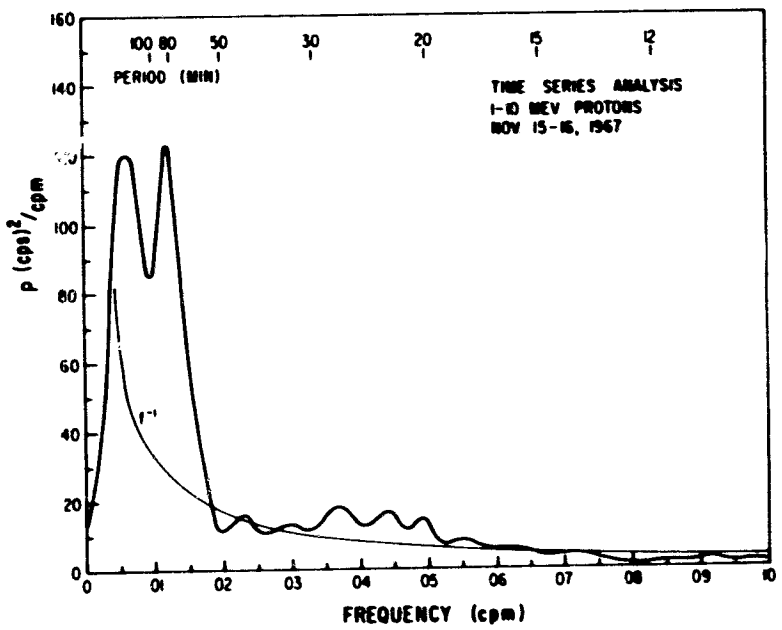
100 80 50 30 20 15 12
PERIOD (MIN)
TIME SERIES ANALYSIS
1-10 MEV PROTONS
NOV 15-16, 1967
p (cpm)²/cpm
160
140
120
100
80
60
40
20
0
f⁻¹
0 01 02 03 04 05 06 07 08 09 10
FREQUENCY (cpm)

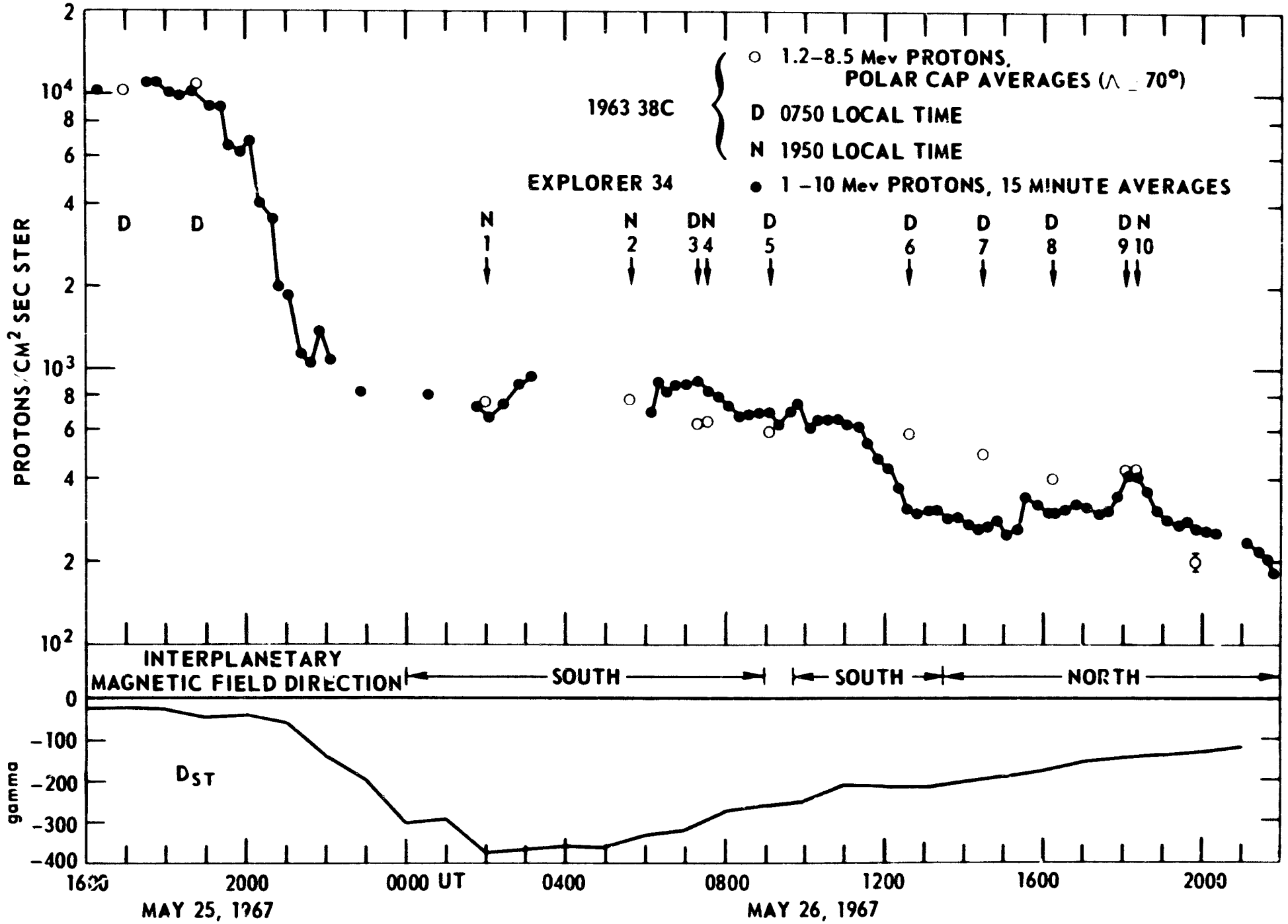
1963 38C
EXPLORER 34
○ 1.2–8.5 Mev PROTONS, POLAR CAP AVERAGES (Λ ≥ 70°)
D 0750 LOCAL TIME
N 1950 LOCAL TIME
● 1 –10 Mev PROTONS, 15 MINUTE AVERAGES
PROTONS/CM² SEC STER
D D N N DN D D D D DN
1 2 3 4 5 6 7 8 9 10
INTERPLANETARY MAGNETIC FIELD DIRECTION
SOUTH
SOUTH
NORTH
gamma
Dst
1600 2000 0000 UT 0400 0800 1200 1600 2000
MAY 25, 1967
MAY 26, 1967

FIGURE

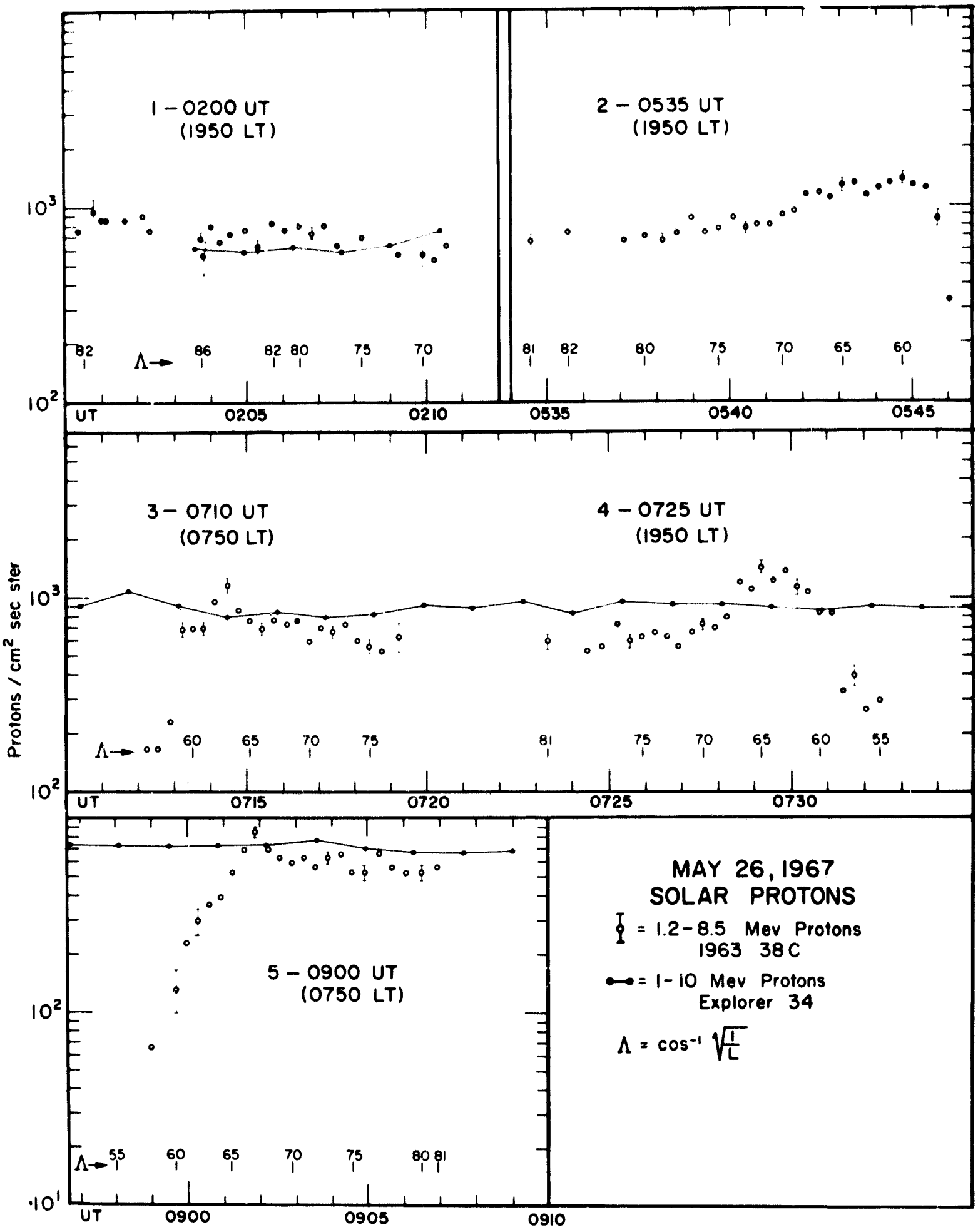
1 – 0200 UT
(1950 LT)
2 – 0535 UT
(1950 LT)
3 – 0710 UT
(0750 LT)
4 – 0725 UT
(1950 LT)
5 – 0900 UT
(0750 LT)
Protons / cm² sec ster
UT
Λ
MAY 26, 1967
SOLAR PROTONS
= 1.2 – 8.5 Mev Protons
1963 38C
= 1 – 10 Mev Protons
Explorer 34
Λ = cos⁻¹ √(I/L)

FIGURE 9

FIGURE

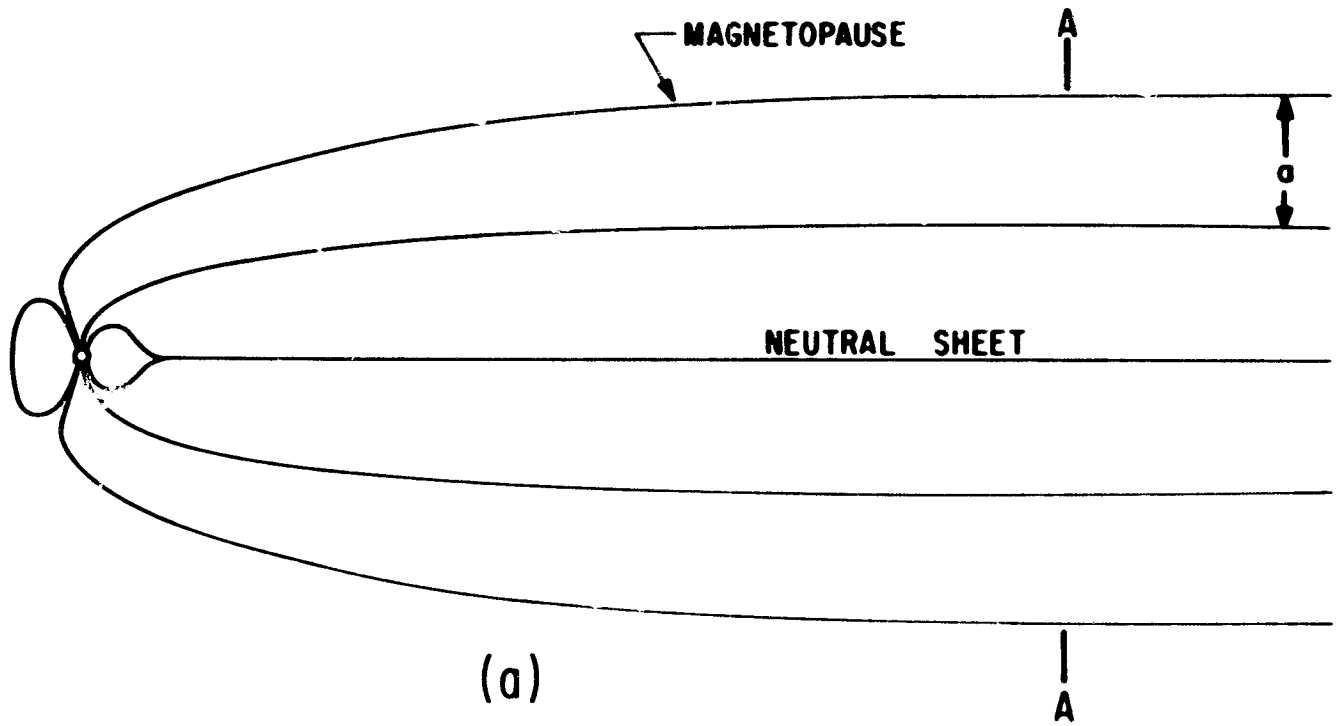

(a)

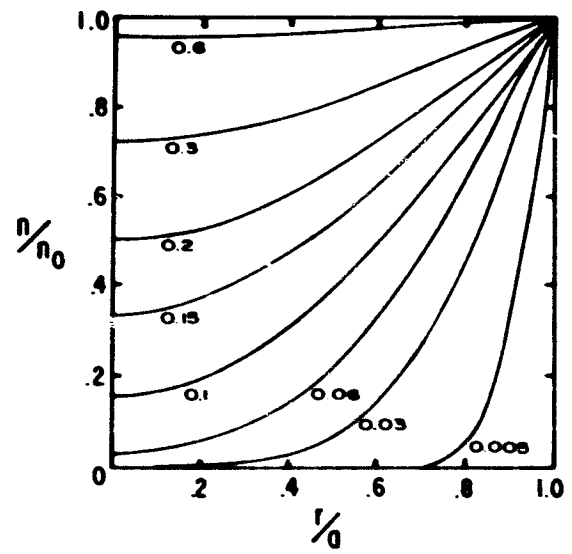

(c)

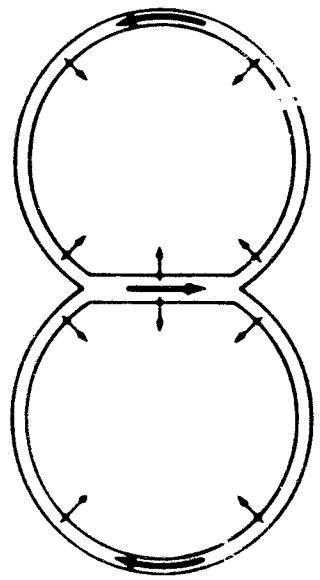

A – A

(b)

SOLAR PROTON FLUXES
1501 – 1511 HOURS, MAY 30 1967
o---o $1.2 \leq E_p \leq 2.2$ MEV, 1963 38C POLAR CAP DATA (1100 km alt.)
●——● $1.0 \leq E_p \leq 10$ MEV, EXPLORER 34 (ALT = 32.6 R_E)

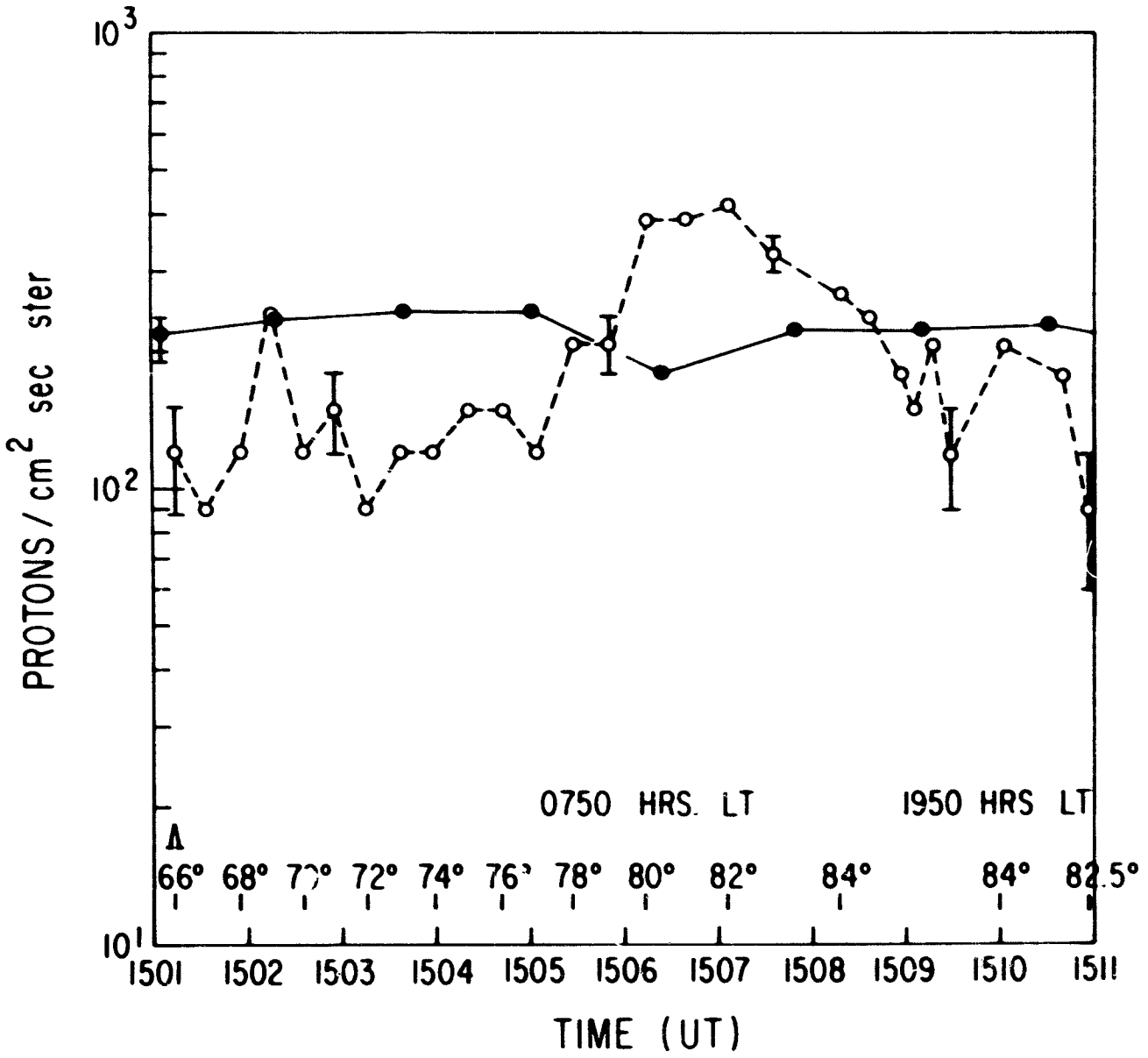

FIGURE 11

X-260-69-202
PREPRINT

NASA TM X-63593

SPACECRAFT PERFORMANCE ANALYSIS

C. V. JUDGE
P. A. VILLONE
W. A. MECCA

MAY 1969

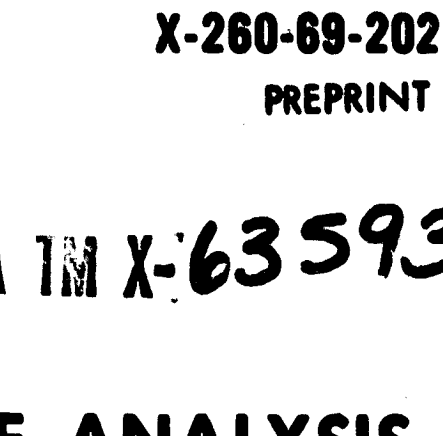

GSFC
GODDARD SPACE FLIGHT CENTER
GREENBELT, MARYLAND

SPACECRAFT PERFORMANCE ANALYSIS

C. V. Judge
Cost Experience Group

P. A. Villone
Business Management Office

W. A. Mecca
Program Support Division

ABSTRACT

The performance lives of a random sample, and of one year design spacecraft, are examined in an effort to provide information concerning the useful life of a spacecraft system exclusive of experiment performance.

CONTENTS

SPACECRAFT PERFORMANCE ANALYSIS

INTRODUCTION

In response to a request to the Program Support Division, the Cost Experience Group of the Business Management Office has investigated performance of spacecraft developed under Goddard management in order to gain insight into the useful life of a spacecraft system exclusive of experiments. The information is intended to aid in amortizating spacecraft costs over an expected useful life, and support the case for demonstrating the potential of long-lived unmanned satellites in the 70's.

The initial analysis attempted to show the progressive growth in performance of satellites in orbit which could be projected. This approach was inconclusive. The approach then turned to utilizing a comparison of the mean design life and mean performance months by year of launch, the separation of follow-on designs as a discrete sample, and the development of a meantime to failure for the spacecraft samples using a reliability calculator based on total performance hours and number of failures.

The initial findings were based on a random sample of twenty-five spacecraft, of which twenty-four provided useful data points. (See Appendix A.) The random sample indicated a 95% confidence for a meantime to failure of 36 months for a 12 month design life follow on satellite.

Due to the limited number of 12 month designs in the original sample, an enlarged sample was sought. An attempt was made to identify the design life of all Goddard managed Spacecraft. Thirty (30) one year design spacecraft were identified and useful performance life was determined from documents and appropriate project personnel.

The results of this analysis support the random sample analysis. The total sample, thirty (30) spacecraft, indicated a Mean Time to Failure (MTF) of thirty-four (34) months at a 95% confidence level and a MTF of thirty-eight (38) months at a 95% confidence level for the follow on design sample consisting of eighteen (18) spacecraft. A follow on spacecraft is considered to be a result of a continuing program using spacecraft designs proven in earlier spacecraft operation.

An attempt to designate a mode of failure was complicated by the "graceful" degrading effect.* The suspected modes of failure will not be presented in this

*Flatow, Fred S., Reliability Assessments for Spacecraft - What Can They Accomplish; GSFC X-301-68-100, March 1968.

document due to their controversial nature and lack of significant contribution to the findings which are directed to "when" a failure, as defined by the criteria for measurement of performance, has occurred rather than the "how" of failure.

CRITERIA FOR MEASUREMENT OF PERFORMANCE

The design life for purposes of this analysis is the design goal or longest period of operation expected at the time of launch as documented in the Project Development Plan (PDP), or other documentation of mission goals and success criteria. When this type of information was not available the existence of a 12 month design goal was confirmed by individuals familiar with the mission, e.g., project manager or other responsible individual involved in the mission.

The analysis is concerned with the operating life of the spacecraft independent of experiment life. To perform this artificial isolation of spacecraft subsystems and experiments those subsystems of the "bus" which provide the environment necessary to support a sensor were selected as the indicators of satisfactory performance. Only spacecraft which obtained orbit were considered in the analysis of performance.

The failure of the control, power, communications or data handling subsystems to provide the designed support for satisfactory operation of a sensor, regardless of the ability of the sensor to function, is considered to be the failure point of the spacecraft in this analysis.

The spacecraft is performing satisfactorily if it is maintaining a satisfactory attitude, temperature, providing power and capable of receiving and transmitting data. A tape recorder failure did not disqualify a spacecraft if useful amounts of real time data can be collected. Spacecraft operation on solar cells at favorable sun angles following loss of battery storage is satisfactory performance when useful amounts of data can be collected.

In the one year design life study, a condition considered a failure for analysis purposes which does not stop transmission of useful data is described as an anomalous operation. The graphical presentations identify anomalous actions by a square (□). Only the performance hours prior to commencement of anomalous operation are used in the MTF analysis on the decay graphs. The OGO series when operating in its spin mode is considered anomalous. The IMP-B operating hours are considered anomalous due to its improper orbit.

The results of the performance life decay graphs and the 95% confidence level of the Mean Time to Failure (MTF) analysis are shown in tabular form in Table I-1. The related graphs and sample descriptions are found in Graphs I-4 through I-7, and Tables I-3 and I-4 respectively.

PART I

SPACECRAFT PERFORMANCE ANALYSIS

OF A RANDOM SAMPLE

PART I

TABLES AND GRAPHS

RESULTS OF ANALYSIS OF THE RANDOM SAMPLE

The analysis presents sample points by comparing performance life to design life, and by examining the follow-on spacecraft as a discrete sample. The data points are developed from Table I-2 (Data Sheet Performing Analysis). The results show that the follow-on spacecraft performance exceeded the first launch spacecraft performance significantly (graph one). The mean performance months to design months ratio has remained between 2.0 and 3.0 while mean design life has increased from 3 months to 9.0 months (graphs two and three).

MEAN TIME TO FAILURE (MTF) ANALYSIS OF THE RANDOM SAMPLE

In order to project the existing data into a measure of Mean Time to Failure a reliability calculator was used.* Given the performance hours and number of failures the calculator fixes a failure rate per cent per 1,000 hours, and a mean time to failure. Confidence levels range from 99% to 50/50 or best estimate. In this analysis the spacecraft is assumed to be the unit under test. Spacecraft which are operating or were turned off while operational are not considered to have failed. Performance hours are measured from day of launch to day of failure or shut down, or to the end of the study period.

The confidence level used in application of this data is a matter of individual choice. For the amortization of cost and consideration given in performance incentives a best guess or 50/50 confidence may be a suitable choice. In the estimation of useful performance in support of a sensor a higher confidence, with resultant reduction in MTF would seem more realistic.

*The reliability calculator used was a circular slide rule as used in test condition environments. The failure rate and Mean Time to Failure (MTF) are computed at the spacecraft level from the total performance hours and the number of spacecraft failures. The validity of the slide rule estimate is tested by establishing approximate confidence intervals in Appendix B.

Table I-1

Summary of Results

Sample and Number of Spacecraft (SC)	Total Performance in Months Σ Performing Months (P)	Total Design Months Σ Design Life (DL)	Mean Performance Months ($\bar{P}$)	Mean Design Life ($\overline{DL}$)	Performance to Design Month Ratio ($\bar{P}/\overline{DL}$)	MTF in Months 95% Confidence	Number of Spacecraft Operating 1-22-69
Random Sample 24 S/C	452.5	225.6	18.8	9.4	2.0:1.0	24	7
Random Sample Follow-on 16 S/C	405.3	129.0	25.3	8.1	3.1:1.0	38	7
12 Mo Design in Random Sample 12 S/C	243.6	144.0	20.3	12.0	1.7:1.0	16.5	4
12 Mo Design Follow-on in Random Sample 7 S/C	215.3	84.0	30.8	12.0	2.6:1.0	27	4

Table I-2

Data Sheet Random Sample Performance Analysis

Flight	Launch Date	Failure Date	Performance Time			Design Life Months	Performance Notes
			Mos	Days	Hrs		
TIROS I	4-01-60	6-16-60	2.5	77	1848	3	1
TIROS III	7-12-61	8-07-62	13	394	9456	3	3
TIROS IV	2-08-62	9- -62	7	203	4872	3	3
OSO I	3-07-62	8-06-63	17	517	12408	6	1-3
SYNCOM I	2-14-63	2-14-63	0	0	0	12	1
TIROS VII	6-19-63	12-06-65	29	903	21672	3	3
SYNCOM II	7-62-63	----	66	2002	48048	12	2
IMP-A	11-27-63	5-06-64	6	164	3936	12	1
IE-A	8-25-64	12-29-64	16	490	11760	12	1
NIMBUS I	8-28-64	9-23-64	1	27	648	[illegible]	1
BE-B	10-10-64	----	51	1561	37464	12	2
BE-C	4-29-65	4-05-68	36	1071	25704	12	
IMP-C	5-29-64	5-12-67	24	714	17136	12	
OGO II	10-14-65	10-24-65	.3	10	240	12	
ESSA II (OT-2)	2-08-66	----	35	1078	25872	6	1-2
OAO I	4-08-66	4-09-66	--	1.5	36	12	
NIMBUS II	5-15-66	1-16-69	32	973	23352	6	
ESSA III	10-02-66	10- -68	24	728	17472	6	
ESSA IV	1-26-67	5- -68	16	462	11088	6	3
ESSA V	4-20-67	----	21	644	15456	6	2

1 - Identifies a first in series spacecraft.
2 - Spacecraft remaining operational as of January 22, 1969.
3 - Spacecraft shut down or no longer monitored as of failure date.

Table I-2 (Continued)

Flight	Launch Date	Failure Date	Performance Time			Design Life Months	Performance Notes
			Mos	Days	Hrs		
IMP-F	5-24-67	----	20	609	14616	12	2
OGO IV	7-28-67	----	18	546	13104	12	2
OSO IV	10-18-67	----	13	462	11088	6	2
TTS-1	12-13-67	5- -68	5	140	3360	12	1

1 - Identifies a first in series spacecraft.
2 - Spacecraft remaining operational as of January 22, 1969.
3 - Spacecraft shut down or no longer monitored as of failure date.

Graph I-1

Mean Satellite Design Life and Performance Life-First Launch Versus Follow-on Satellites

Graph 1 compares the mean performance life to the mean design life of the first S/C in any launch series to the performance of life of the remaining S/C.

Satellites First in Series	Follow-on Satellites
TIROS I	TIROS III
OSO I	TIROS IV
SYNCOM I	TIROS VII
IMP-A	SYNCOM II
IE-A	BE-B
NIMBUS I	BE-C
OAO I	IMP-C
TTS I	OGO II
	ESSA II (OT-2)
	NIMBUS II
	ESSA III
	ESSA IV
	ESSA V
	IMP-F
	OGO IV
	OSO IV

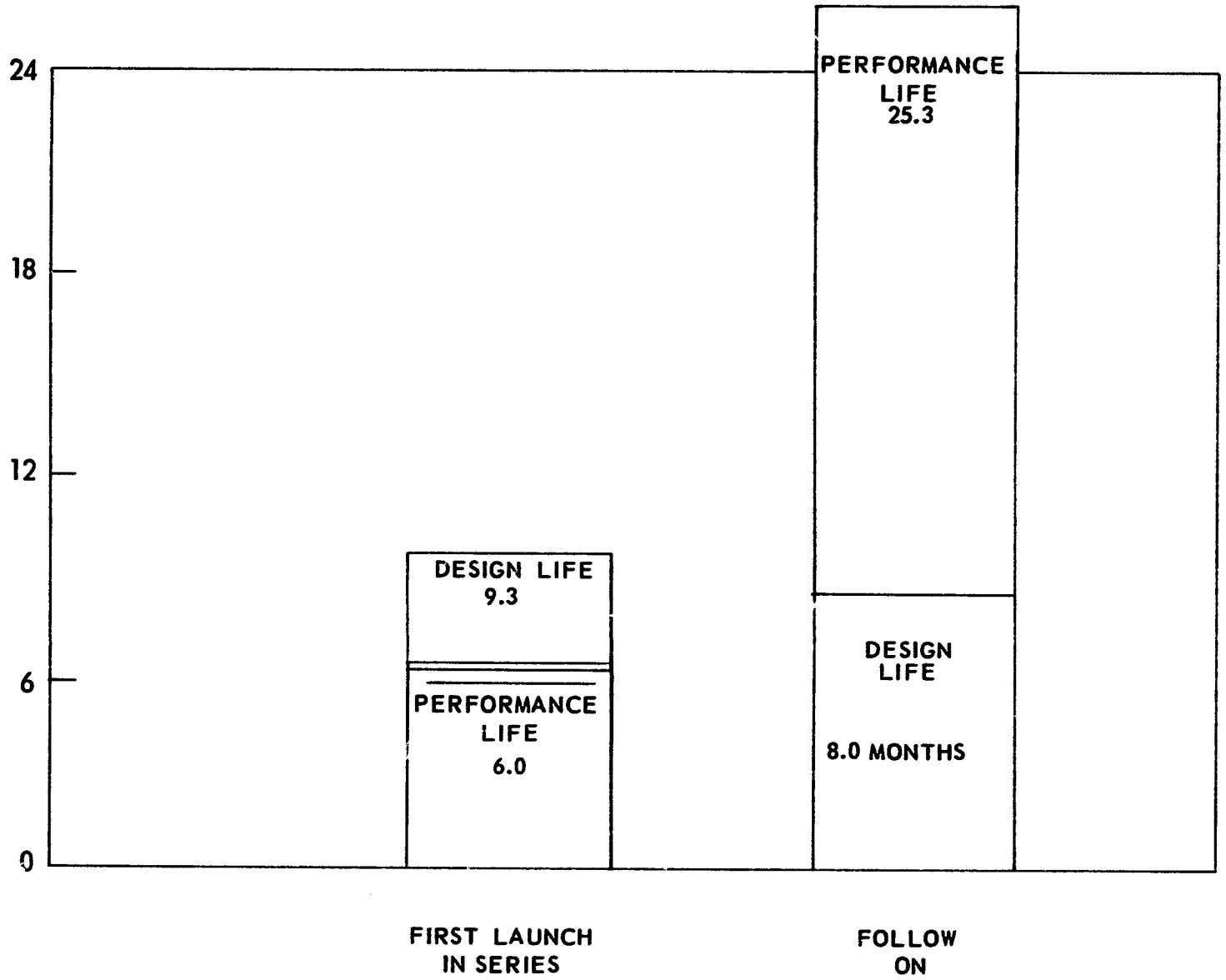

Graph 1-1. Mean Satellite Design Life and Performance Life First Launch vs Follow On Satellite

Graph I-2

Satellites Lifetime in Orbit

The mean design life for satellites launched in 1961 through 1967 is compared to the mean performance life by year. Operational satellites remain as follows:

1 each from Cy 63, 64, 66

4 from CY 67

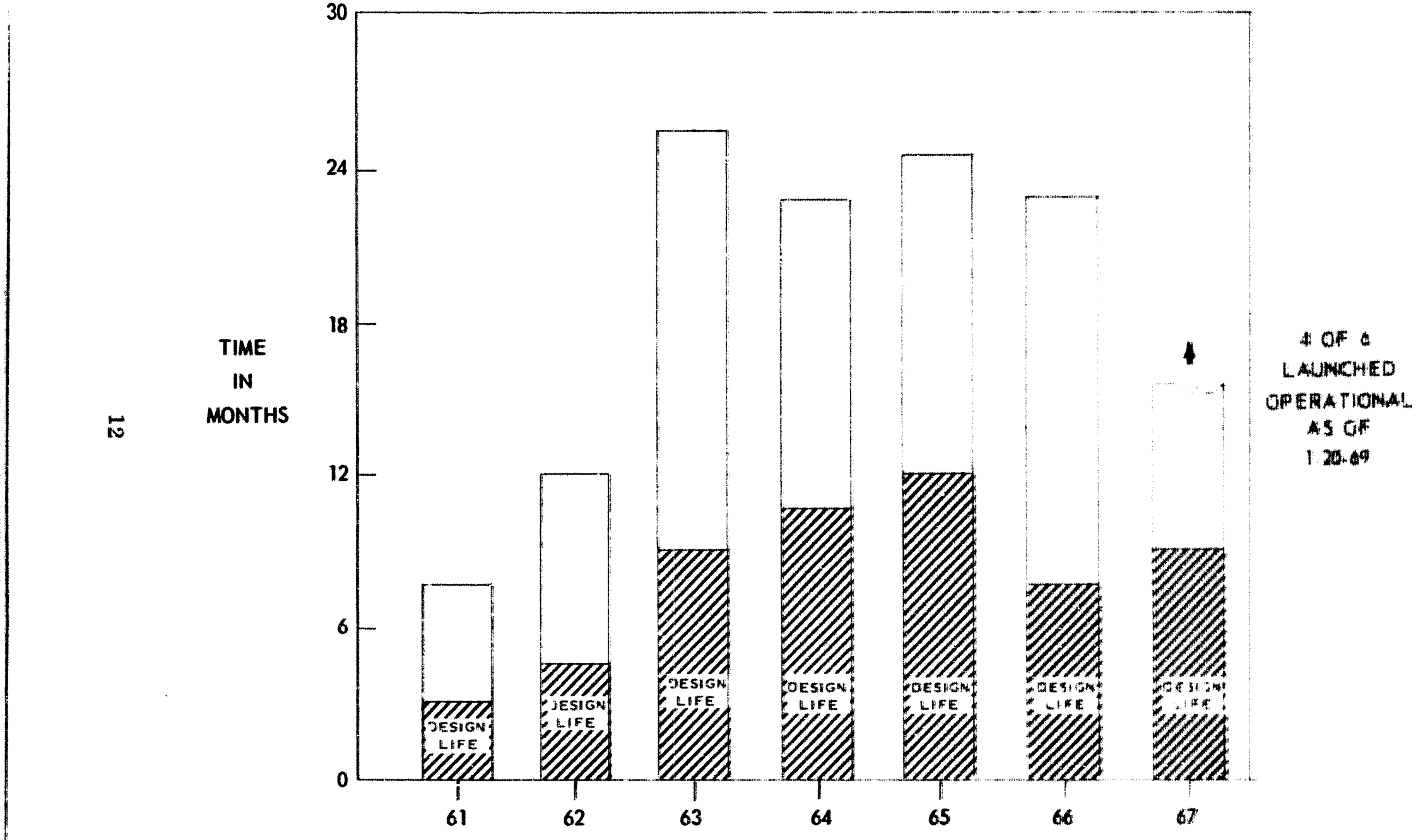

Graph I-2. Satellites Mean Lifetime in Orbit by Year of Launch

Graph 1-3

Mean Satellite Performance Months ÷ Mean Design Life by Year of Launch

Graph 3 is a plot of the mean performance design life ratio for sample satellites by year of launch.

Four of the six satellites in the CY 67 launch group are still operational. One S/C each in CY 63, 64, and 66 is operational.

CY 65 performance design life ratio was lowered due to the failure of the OGO II control system ten days after launch. While OGO II is still operational in its backup spin mode, it is considered a failure in the sample due to the existence of experiments requiring a stable platform in its payload.

CY 64 performance design life ratio is lowered by NIMBUS I.

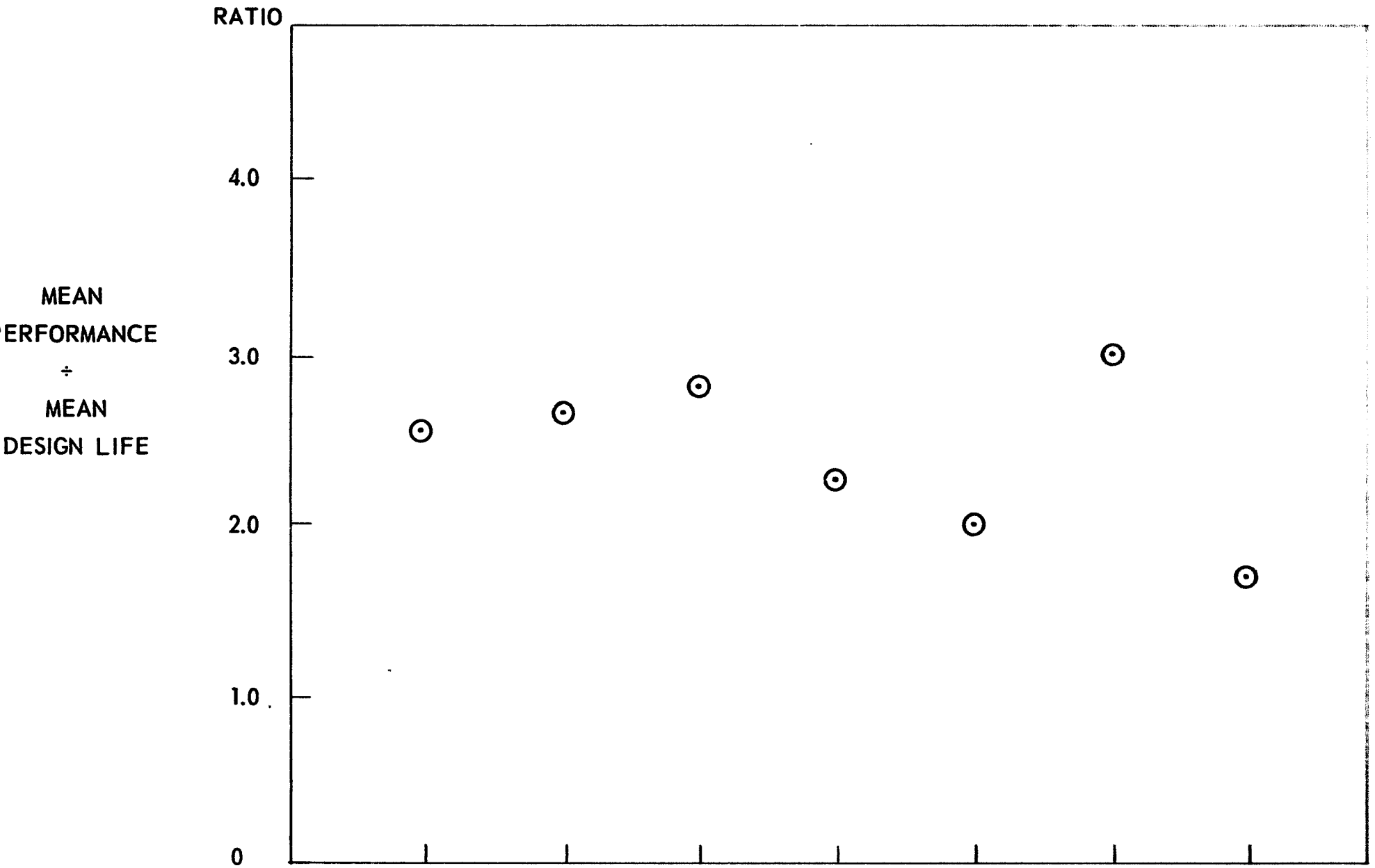

Graph I-3. Mean Satellite Performance Mean Design Life

Graph I-4

Performance Life Decay Random Sample

This graph compares the sample mean design life, 9.4 months, to the months performed by spacecraft in the sample. The area to the left of the design life line is 225.6 months (9.4 × 24 = 225.6). The area under the performance line is 452.5 months. Performance to design life ratio is 2.0. It should be noted that at the end of the sample period, January 22, 1969 there were seven operational spacecraft.

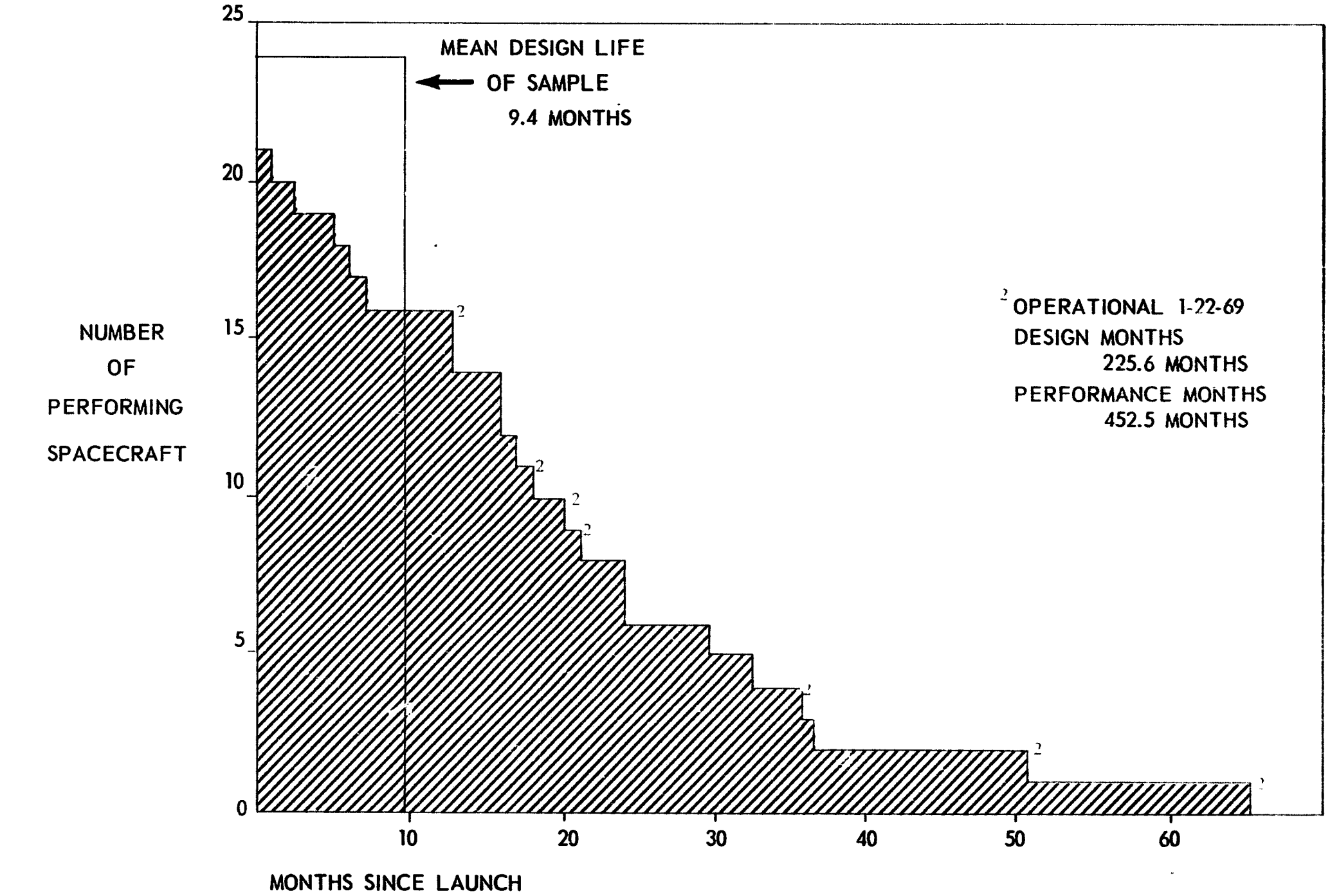

Graph I-4. Performance Life Decay Random Sample

Graph I-5

Performance Life Decay of Follow-on Missions

This sample represents the performance in months from date of launch for the sixteen follow-on spacecraft. At the end of the sample period, January 22, 1969, seven spacecraft remained operational. The performance months design months ratio is 3.1:1.0 as of January 22, 1969.

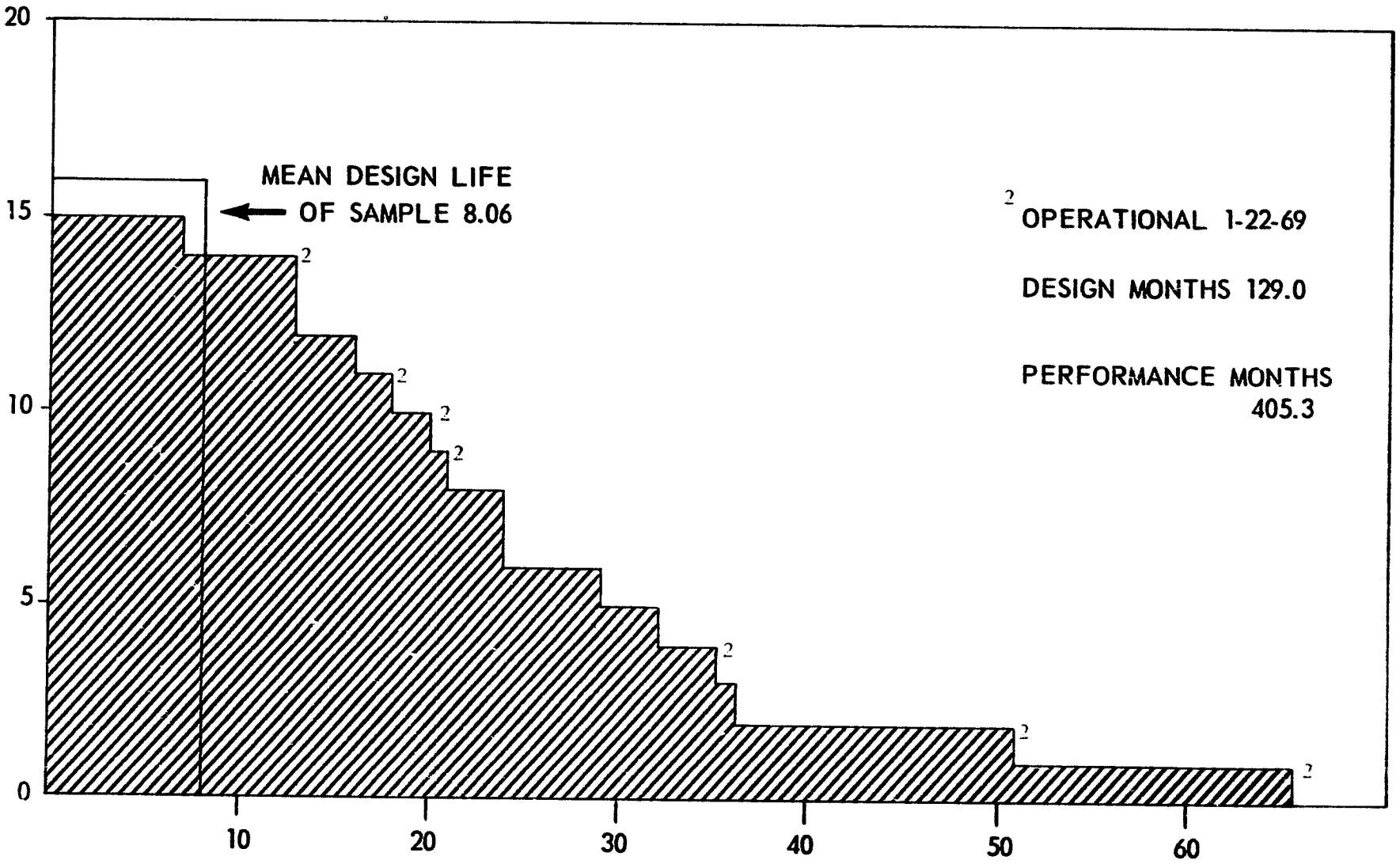

Graph I-5. Performance Life Decay Follow On Missions

Graphs I-6 and I-7

Performance Life Decay of One Year Design Life and One Year Design Follow-on Spacecraft

The random sample contains twelve one year design satellites of which seven are follow-on spacecraft. The performance month design month ratio for the one year design sample is 1.7:1.0. The follow-on performance month design month ratio for the follow-on spacecraft is 2.6:1.0.

The size of the sample was considered marginal for use in the analysis, therefore, a new sample of all identifiable one year designs is examined in Part II.

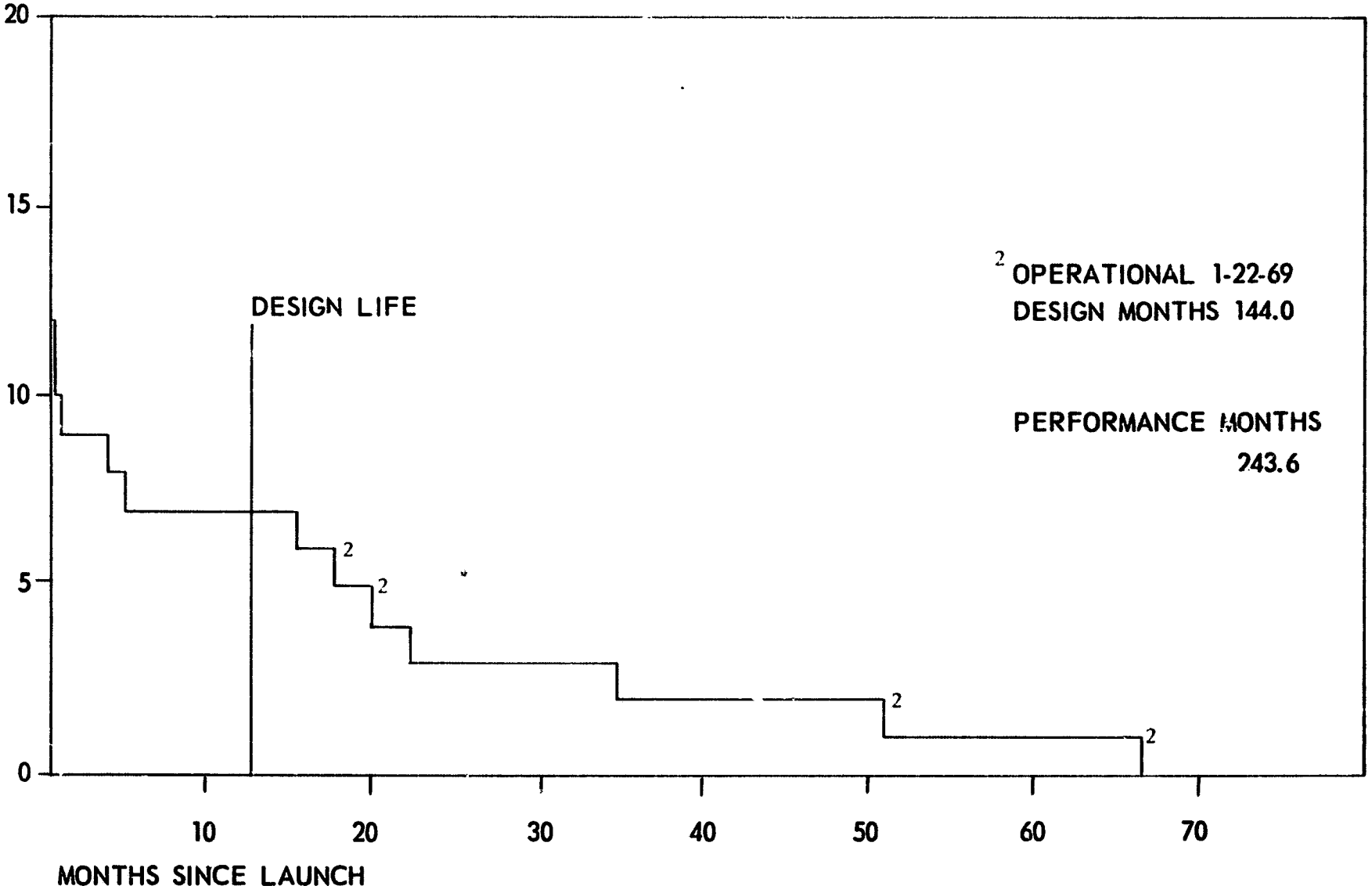

Graph I-6. Performance Life Decay One Year Design

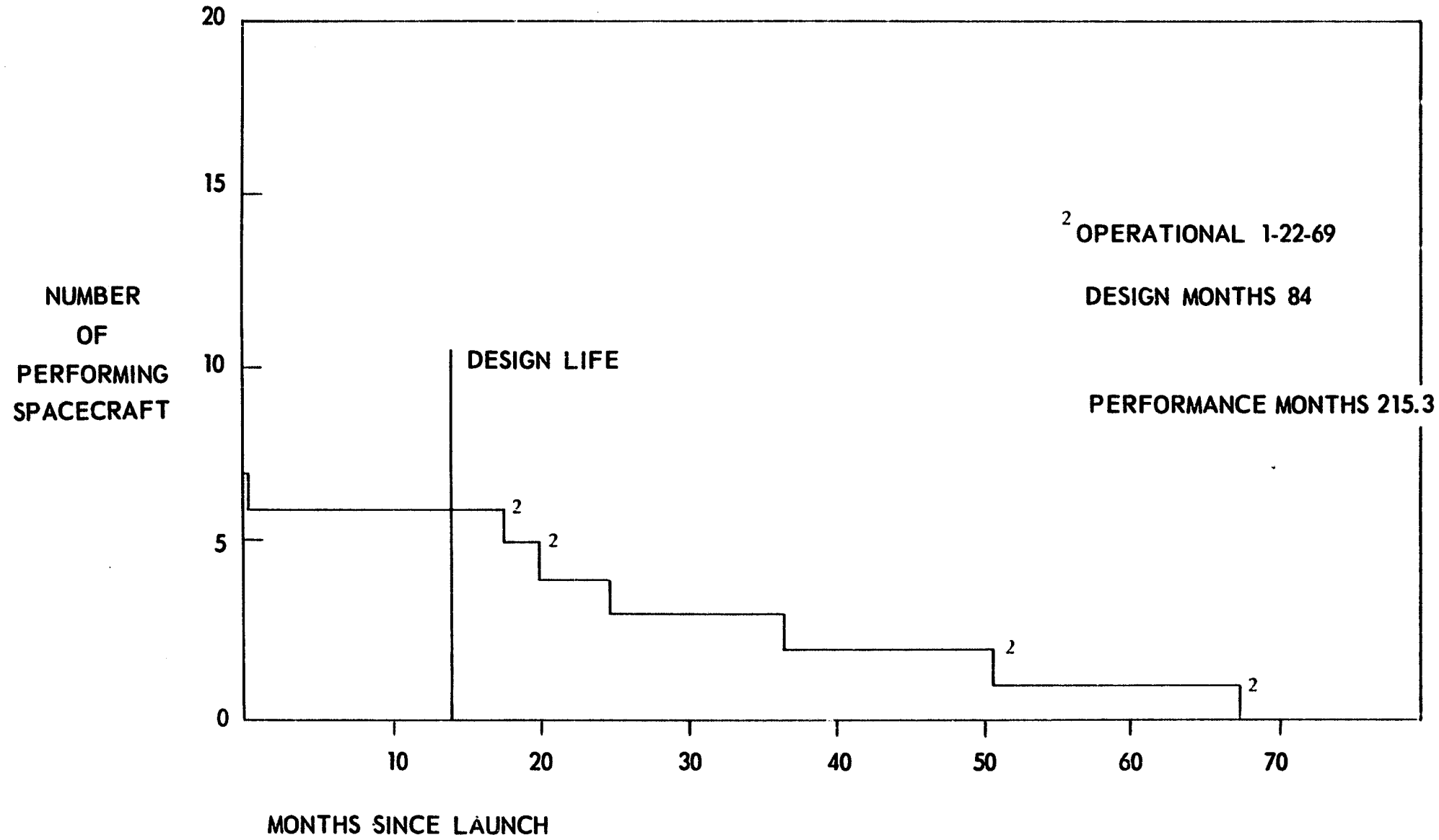

Graph I-7. Performance Life Decay One Year Design Follow On

Table I-3

Mean Time to Failure Analysis

Total Performance Hours - 330,636	
Number in Sample - 24	
Number of Failures - 12	Other S/C in Sample - 12
TIROS I#1	TIROS III
SYNCOM I#1	TIROS IV
IMP-A#1	OSO I#1
IE-A#1	TIROS VII
NIMBUS I#1	SYNCOM II*2
BE-C	BE-B*2
IMP-C	ESSA II*2
OGO II	ESSA IV
OAO I#1	ESSA V*2
NIMBUS II	IMP-F*2
ESSA III	OGO IV*2
TTS-1#1	OSO IV*2

Confidence Level	MTF Hours	Months	Failure Rate % Per 1,000 Hrs.
99	14,700	20.4	6.8%
95	17,500	24.3	5.7%
90	18,900	26.3	5.3%
60	25,000	34.7	4.0%
50/50	26,900	37.3	3.7%

1. # First spacecraft in series.
2. * Operational spacecraft at end of sample period January 22, 1969.

Table I-4

Mean Time to Failure Analysis

Follow-on missions only	
Performance hours - 296,640	
Number of Failures - 5	Other S/C in Sample - 11
BE-C	TIROS III
IMP-C	TIROS IV
OGO II	TIROS VII
NIMBUS II	SYNCOM II*[2]
ESSA III	BE-B*[2]
	ESSA II*[2]
	ESSA IV
	ESSA V*[2]
	IMP-F*[2]
	OGO IV*[2]
	OSO IV*[2]

Confidence Level	MTF Hours	Months	Failure Rate % Per 1,000 Hrs.
99	22,900	31.8	4.4%
95	27,900	38.8	3.5%
90	32,000	44.4	3.1%
60	47,000	65.3	2.1%
50/50	51,000	70.8	1.9%

2. * Operational spacecraft at end of sample period January 22, 1969.

PART II

SPACECRAFT PERFORMANCE ANALYSIS

OF

ONE YEAR DESIGN SPACECRAFT

PART II

TABLES AND GRAPHS

ONE YEAR DESIGN LIFE SAMPLE

The one year design sample consists of thirty (30) one year design spacecraft. The sample consists of all Goddard Managed one year design life spacecraft for which design life and performance life could be fixed with reasonable accuracy.

The performance time is measured to a failure. A failure is the result of the control, power, communications, or data handling subsystems inability to provide the designed support for satisfactory operation of a sensor, irregardless of the ability of the sensor to function.

Total performance hours are noted in Table II-2. The performance hours including anomolous hours are shown separately for information only. The anomalous operation hours were not used in the MTF analysis or reflected in the graphical analysis.

The anomalous performance identified in Table II-2 and on the graphical analysis identifies a situation in which data collection from the spacecraft continued but performance was not adequate for the analysis. The OGO anomaly is the collection of data in the "backup" or spin-mode which does not provide designed support for satisfactory operation of all sensors. The IMP-A collected small amounts of useful data from May 30, 1964 to May 10, 1965 when at favorable sun angles. The IMP-B gathered useful data from October 4, 1964 to July 18, 1965 but the mission was classified as a failure due to improper orbit as a result of launch vehicle malfunction.

ANALYSIS OF ONE YEAR DESIGN SAMPLE

In the analysis of one year design, a conservative bias has been effected by the Criteria for Measurement of Performance. The exclusion of performance hours of the OGO in the spin mode, the exclusion of data from IMP-A following battery failure, and IMP-B in total due to improper orbit result in a reduction of 127 performance months in the analysis of performance of 12 month design spacecraft.

The mean performance in months has exceeded the design life consistently since 1962. The percentage of launched spacecraft remaining operational is 45% for all years after 1964 with no less than 40% remaining operational in each year since 1964.

The performance life decay graphs show a tendency for the spacecraft failure rate to decrease after an initial period of about six months from launch.

The initial or infant mortality in the first month accounted for 20% of the observed failures or anomalous occurrences in the sample. An additional 27% of the observed failures and anomalies occur in the next five months. A total of 47% of all observed failures or anomalies occur in the first six months following launch. During the remaining six months of the design life only 6.6% of the failures or anomalous occurrences were observed. The high initial mortality is not exhibited by the follow-on sample.

The results of the performance life decay graphs and the 95% confidence level of the Mean Time to Failure (MTF) analysis are shown in Table II-1. The related graphs and sample descriptions are found in Graphs II-3 and II-4 and Tables II-3 and II-4 respectively.

Table II-1

Summary of Results

Sample and Number of Spacecraft (SC)	Total Performance in Months Σ Performing Months ($\hat{P}$)	Total Design Months 30 × 12 (DL)	Mean Performance Months (1/2) ($\bar{P}$)	Mean Design Life ($\overline{DL}$)	Performance to Design Month Ratio ($\bar{P}/\overline{DL}$)	MTF in Months at 95% Confidence	Number of Spacecraft Operations 3-11-69
One Year Design 30 S/C	756	360	25.2	12	2.1:1.0	34	13
Follow-on Mission 18 S/C	517	216	28.7	12	2.4:1.0	39	10

Table II-2

Data Sheet for Twelve Month Design Sample

Spacecraft	Launch Date	Failure Date	Performance		Performance Notes
			Month	Hours	
Explorer VII	10-13-59	8-24-61	22	16344	1
Explorer XII	8-15-61	12-06-61	4	2736	1
Ariel I	4-26-62	11-09-64	31	22320	1, 3
Alouette I	9-28-62	----	77	56640	1, 2
Relay I	12-13-62	8- -65	32	23256	1
Syncom II	7-26-63	----	67	46992	2
(IMP-A) Explorer XVIII	11-26-63	5-30-64	6	4536	4
Relay II	1-21-64	----	62	42576	2
Ariel II	3-27-64	3- -66	24	17520	3
Syncom III	8-19-64	----	54	40080	2
(IE-A) Explorer XX	8-25-64	12-29-65	16	11760	1
OGO I	9-04-64	9-04-64	0	5	1, 4
(BE-B) Explorer XXII	10-09-64	----	52	38784	2
(S-3C) Explorer XXVI	12-21-64	5-26-67	29	21216	
(BE-C) Explorer XXVII	4-29-65	4-05-68	35	25944	
(IMP-C) Explorer XXVIII	5-29-65	5-12-67	24	17136	
OGO II	10-14-65	10-23-65	0	240	4
Alouette II	11-29-65	----	39	28800	2
(DMEA) Explorer XXXI	11-29-65	----	39	28800	2
OAO I	4-08-66	4-09-66	0	36	1
(AE-B) Explorer XXXII	5-25-66	3-22-67	10	7104	
OGO III	6-07-66	8-23-66	3	2040	4
AIMP-D	7-01-66	----	31	23736	2
ATS-1	12-06-66	----	27	19872	1, 2, 5

Table II-2 (Continued)

Spacecraft	Launch Date	Failure Date	Performance		Performance Notes
			Month	Hours	
(IMP-F) Explorer XXXIV	5-24-67	----	21	15816	2
(AIMP-E) Explorer XXXV	7-19-67	----	19	14520	2
OGO IV	7-28-67	1-19-69	19	13008	3, 4
ATS III	11-05-67	----	16	11856	2
TTS I	12-13-67	5- -68	5	3360	1
OGO V	3-04-68	----	12	8952	2

Performance Notes:

1. First spacecraft in series.
2. Spacecraft remains operational as of March 11, 1969.
3. Spacecraft shut down or no longer tracked as of failure date shown.
4. Spacecraft exhibited anomalous performance after failure date shown. Total measurable performance for anomalous spacecraft is as follows:

Spacecraft	Launch Date	Total Measured Performance	Performance	
			Months	Hours
(IMP-A) Explorer XVIII	11-26-63	5-10-65	18	12792
OGO I	9-04-64	----	52	39624
IMP B	10-04-64	7-18-65	9	6960
OGO II	10-14-65	11-01-67	25	17976
OGO III	6-07-66	----	32	24240
OGO IV	7-28-67	----	19	13992

5. ATS series design life exceeds 12 months but has been used as 12 months for purpose of this analysis.

Graph II-1

Twelve Month Design Life

Mean Performance in Months
vs.
Year of Launch

The OGO anomalous hours are not shown in 1964, 1965, and 1966. The 1966 performance months are also affected by the OAO I failure at launch.

The year of launch mean performance has exceeded the design life of 12 months in all samples. The 1959-1961 sample of two spacecraft is not considered to be significant due to the lack of complete documentation on design life criterion.

As a result of the MTF analysis, the spacecraft remaining operational in the 1966 and 1967 samples have a 99% confidence of reaching a 29 month performance level.

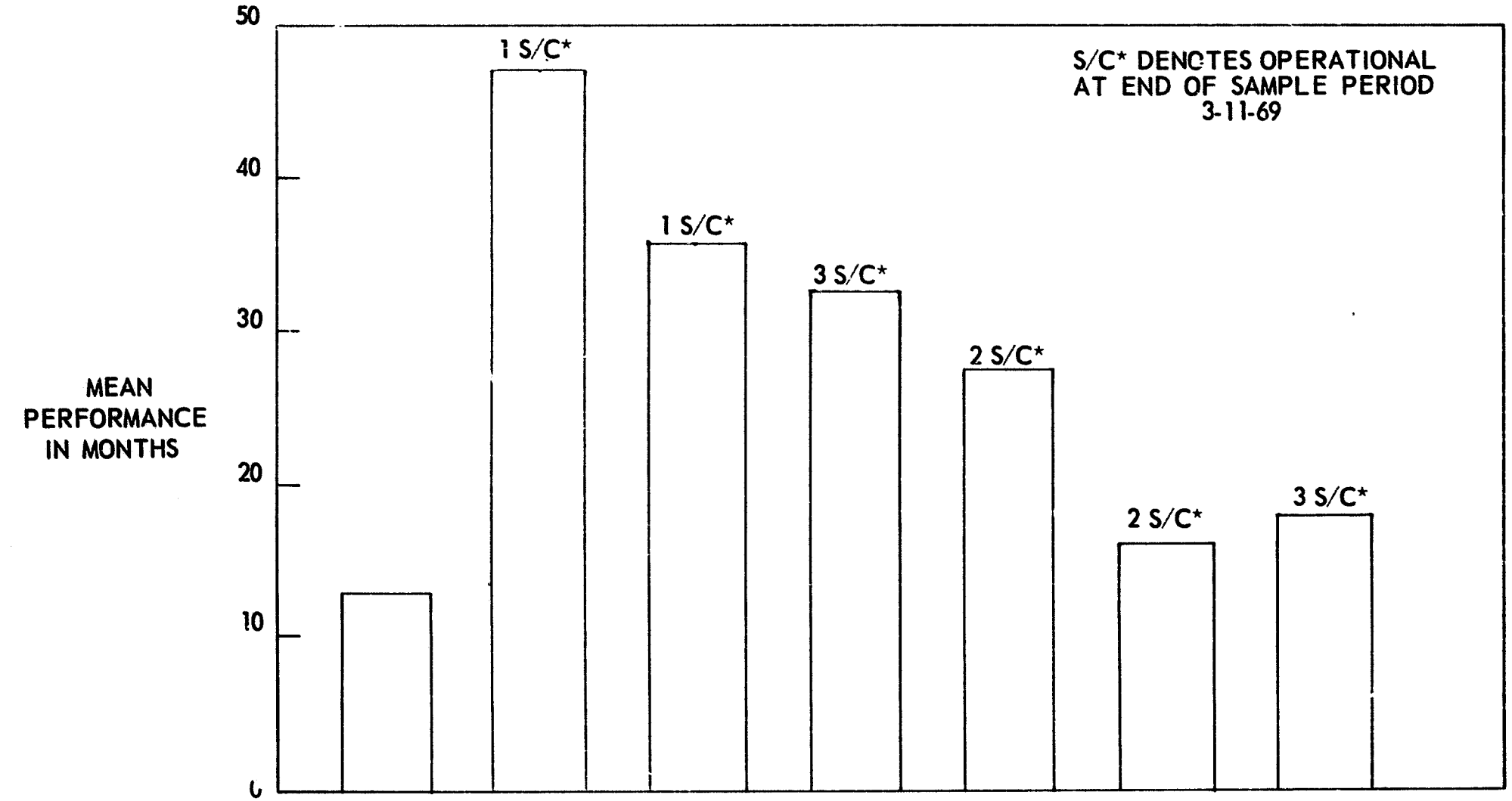

YEAR OF LAUNCH	59 to 61	62	63	64	65	66	67
TOTAL Performance Months	26	140	73	237	137	71	80
NUMBER LAUNCHED	2	3	2	7	5	5	5

Graph II-1. Mean Performance in Months vs Year of Launch

Graph II-2

Twelve Month Design Life

Mean Performance Design Life Ratio by Year

The remarks concerning anomalous hours from Graph II-1 are also true in this presentation.

The overall ratio of 2.1:1.0 is developed from Graph II-3. The follow-on ratio for all years which is not shown is 2.4:1.0 is developed from Graph II-4.

The results of the MTF analysis indicate a 90% confidence level in the launch year samples 1965, 1966 and 1967 mean performance design life ratio ($\bar{P}$/DC) reaching the 3.0 level.

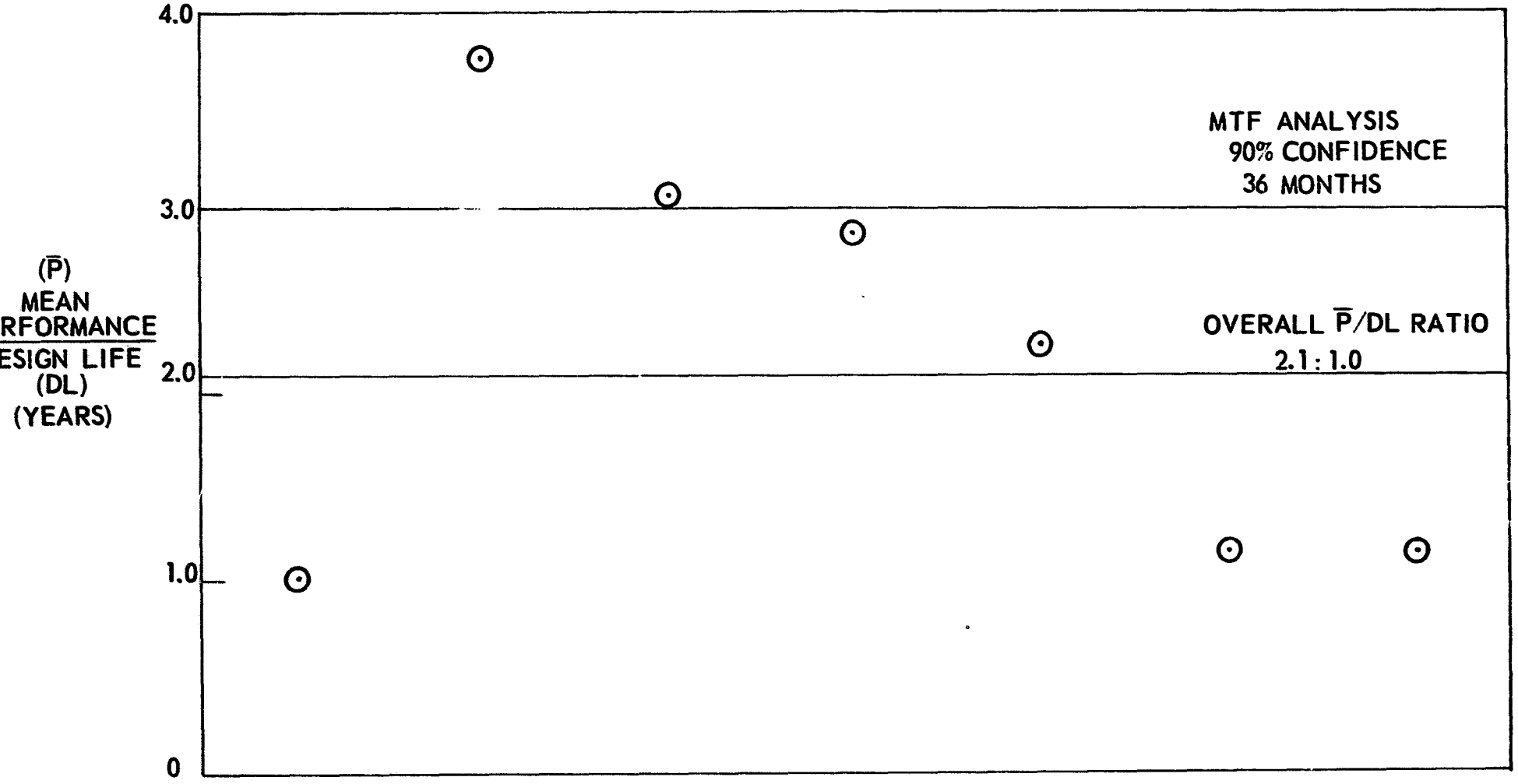

YEAR OF LAUNCH	1959-61	62	63	64	65	66	67
% OPERATIONAL	0	33	50	42	40	40	60
S/C REMAINING OPERATIONAL	0	1	1	3	2	2	3

Graph II-2. Mean Performance Design Life Ratio by Year

Graph II-3

Twelve Month Design Life

Number of Spacecraft Performing
vs.
Months Since Launch

The tendency of spacecraft failure rate to decrease after an initial period of about six months is shown on this graph. The initial or infant mortality in the first month accounts for 20% of all the failures or anomalous occurrences. An additional 26.6% of the failures or anomalous events occur prior to reaching six months in orbit.

The MTF lines represent the expected sample MTF at the indicated level of confidence.

The Performance month to Design month ratio (P/DL) for the sample is 2.1:1.0 as of March 11, 1969.

The mean performance months as of March 11, 1969 are 25.2 months.

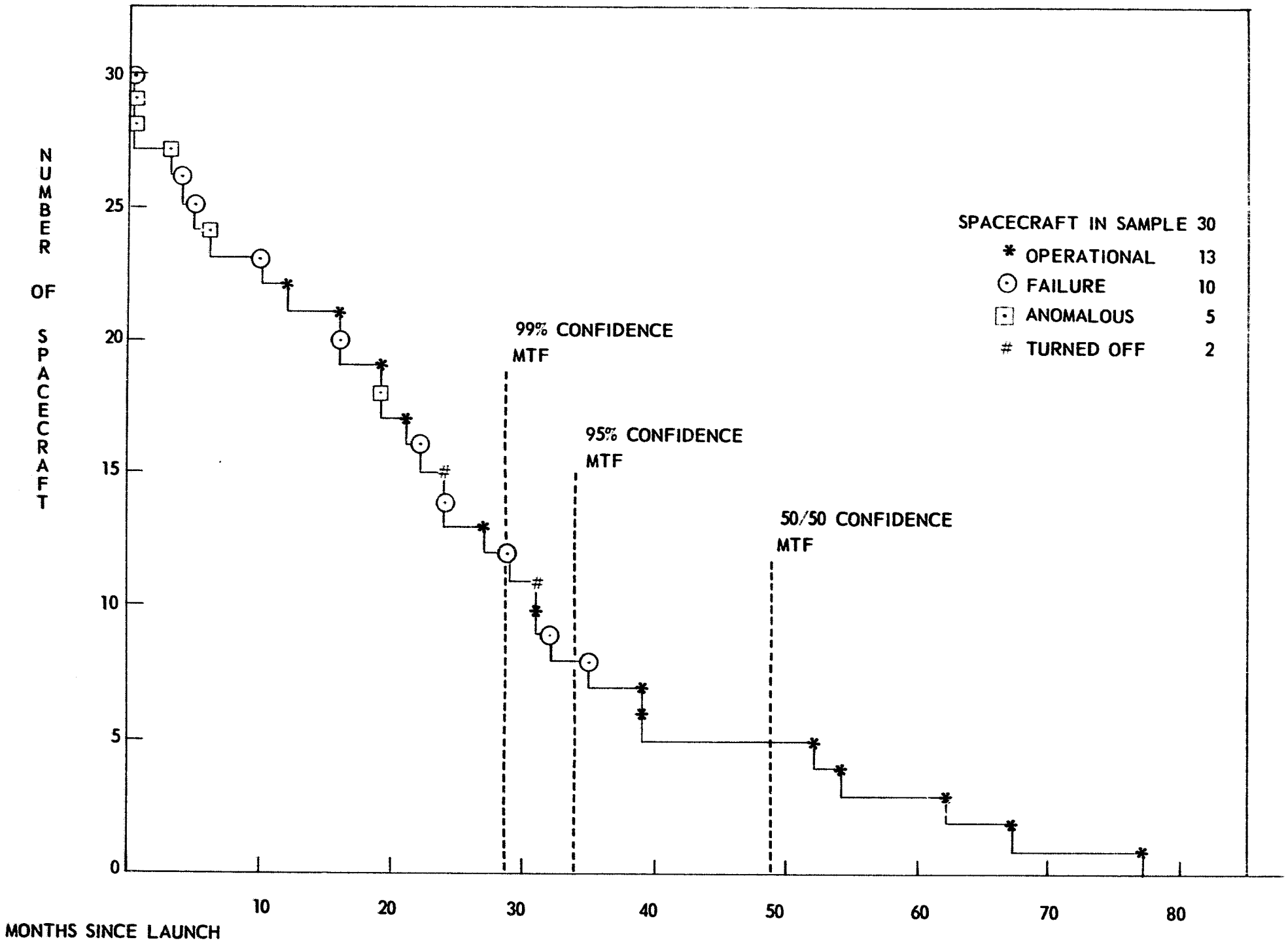

Graph II-3. Number of Spacecraft Performing vs Months Since Launch

Graph II-4

Twelve Month Design Life

Follow-on Spacecraft Performing
vs.
Months Since Launch

The follow-on spacecraft failure rate does not exhibit the high infant mortality of the total sample. With the exception of the OGO which is considered anomalous and the Explorer XXXII (AE-B) all spacecraft have met or exceeded the design life criteria.

The MTF lines represent the expected sample MTF at the indicated level of confidence.

The Performance months to Design months ratio (P/DL) for the sample is 2.4:1.0.

The mean performance months (P/SC) as of March 11, 1969 are 28.7 months.

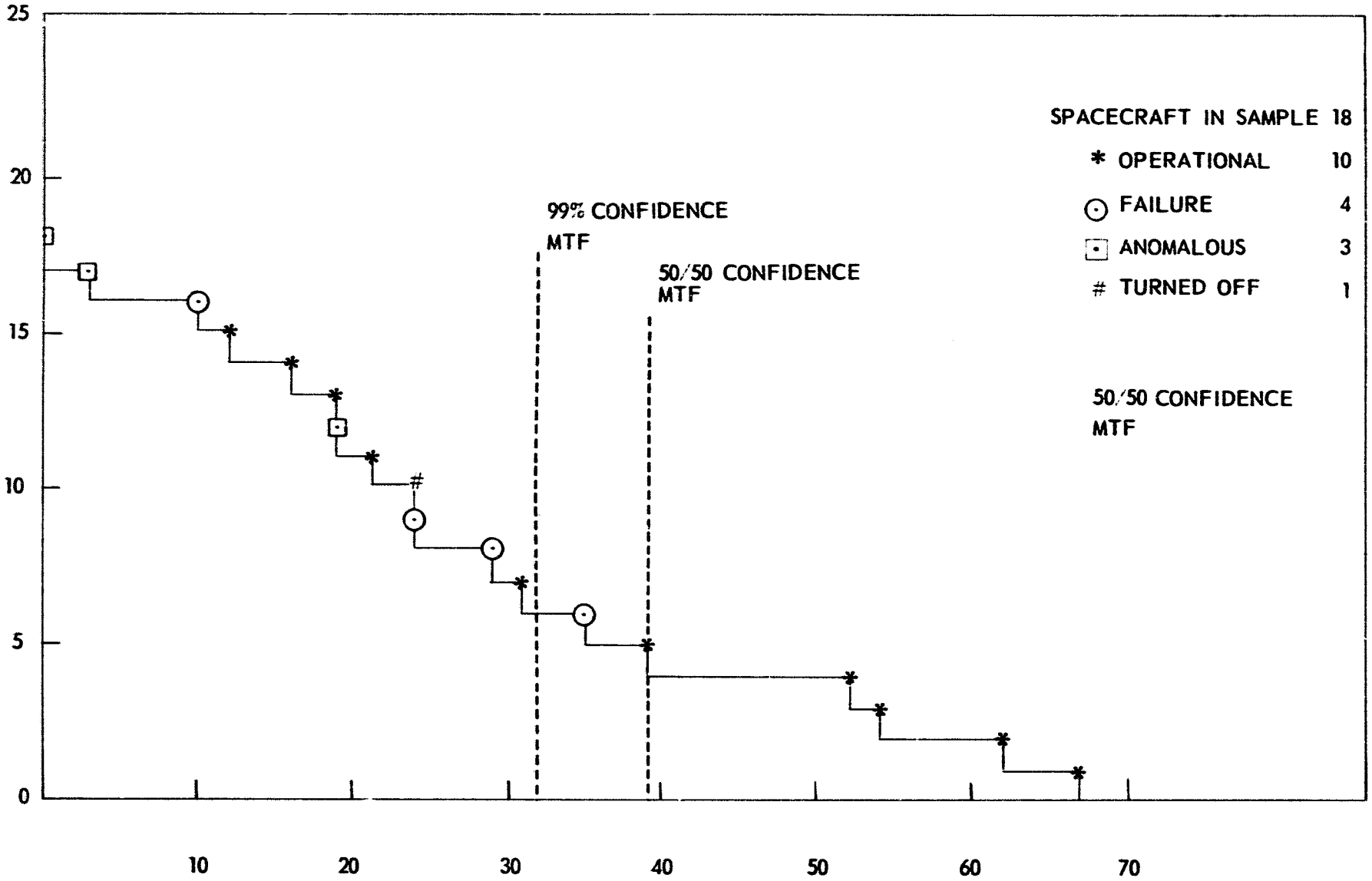

Graph II-4. Follow On Spacecraft Performing vs Months Since Launch

Table II-3

Mean Time to Failure Analysis

Total Performance Hours - 565,985	
Number in Sample - 30	
Number of Failures - 15	
Explorer VII Explorer XII Relay I Explorer XVIII OGO I Explorer XXVI Explorer XX Explorer XXVII	Explorer XXVIII OGO II OAO I Explorer XXXII OGO III OGO IV TTS I

Confidence Level	MTF Hours	Months	Failure Rate % Per 1,000 Hrs.
99	21,000	29	4.7%
95	24,500	34	4.1%
90	26,200	36	3.8%
60	33,500	46	2.9%
50/50	36,000	49	2.7%

Table II-4

Follow-on
Mean Time to Failure Analysis

Total Performance Hours - 376,320
Number in Sample - 18
Number of Failures - 7
Explorer XXVI Explorer XXVII Explorer XXVIII OGO II Explorer XXXII OGO III OGO IV

Confidence Level	MTF Hours	Months	Failure Rate % Per 1,000 Hrs.
99	23,800	32	4.2%
95	28,500	39	3.5%
90	32,000	44	3.1%
60	45,000	62	2.2%
50/50	48,800	66	2.0%

APPENDIX A

RANDOM SAMPLE SELECTION PROCEDURE

Forty-six two digit numbers were selected from the first two digits of a one-hundred line fourteen column five digit random number table. Entry to a line and column was made by using two digits in the table. Columns were read down five digits, then diagonally to the next block of fives. Five entries were made to complete the sample.

Random digits were matched to launch sequence numbers to select S/C. Launch sequence numbers are chronologically assigned in "GSFC Space Program Record: August 1959 to December 31, 1967. (PEP - 067), GSFC, NASA; Greenbelt, Maryland. Twelve random digits greater than seventy-three and eight duplications were eliminated from the sample. Three launch vehicles failed. These sample numbers were replaced by the next numerical launch not already in the sample. The Telstar, launch twenty-two, was eliminated as non-Goddard Managed. Launch seventy-three carried two S/C, TTS-1 and Pioneer VIII. Pioneer VIII was eliminated as non Goddard Managed. The resulting sample is twenty-five S/C in the following programs:

Missions in sample of twenty-five

Program	Number in Sample	Mission
PIONEER	1	V
TIROS	4	I, III, IV, VII
OSO	2	I, IV, (D)
SYNCOM	2	I, II
EXPLORER	6	XVIII (IMP-A), XXVIII (IMP-C), XXXIV (IMP-F), XX (S-48) XXII (BE-B), XXVII (BE-C)
NIMBUS	2	I, II
OGO	2	II, IV (POGO) (D)
ESSA	1	2 (OT-2)
ESSA	3	III (TOS-A), IV (TOS-B) V (TOS-C)

Program	Number in Sample	Mission
OAO	1	I
TTS	1	I
TOTAL	25	

It should be noted that only four of the sixty-six missions successfully orbited were classifed as mission failures. Three of the four appeared in the random sample. The only unsuccessful mission not in the sample is OGO I.

The analysis of performance is based on twenty-four of the twenty-five spacecraft. The PIONEER V mission could not be included due to a lack of available data.

APPENDIX B

CHI-SQUARE CONFIDENCE INTERVAL TEST OF RELIABILITY CALCULATOR

The purpose of this appendix is to demonstrate a method which may be used in establishing approximate intervals for (1) the Mean Time to Failure (MTF) calculations and (2) to test the validity of the reliability calculator circular slide rule in developing Mean Time to Failure (MTF) calculations for the analysis.

It is assumed that an expotential model of the failure-time distribution is given by

$$f(t) = \alpha e^{-\alpha t} \qquad t > 0, \quad \alpha > 0$$

The spacecraft is the component under life test, not the related subsystems. The value of α is an assumed constant failure rate representative of the failure period which occurs following infant mortality and prior to wear out failures. The test life of the component is from launch to failure or to the end of the observation period. Spacecraft which were shut down by command were not considered to have failed.

To make inferences concerning the mean life (μ) of the spacecraft and the validity of the reliability calculator, the assumptions are an expotential model of the failure-time distribution, a fixed accumulated amount of life time (T) elapsed, and the observed number of failures (k) may be treated as the value of a random variable.

Given the above condition, an approximate confidence interval for the mean life of the spacecraft is given by

$$\frac{2T}{\chi_4^2} < \mu < \frac{2T}{\chi_3^2}$$

When T = Total observed performance hours at the end of the sample period.

μ = The mean time to failure.

Where χ_4^2 cuts off a right hand tail of area /2 under the Chi-square distribution with 2k + 2 degrees of freedom, and χ_3^2 cuts off a left hand tail of area /2 under the Chi-square distribution with 2k degrees of freedom.*

The sample examined was the twelve month design life follow-on spacecraft (Table II-4). Based on the results of the analysis (shown in Table B-1) for the conditions assumed the circular slide rule MTF estimates are considered valid.

*p. 375, Miller, I. and Freud, John E., Probability and Statistics for Engineers, Prentice Hall, Inc., Englewood Cliffs, N. J., 1965.

Table B-1

Chi-square Confidence Level Estimates of Assumed Mean Time to Failure for Twelve Month Design Follow-on Spacecraft

$$\frac{2T}{\chi_4^2} < \mu < \frac{2T}{\chi_3^2}$$

Confidence Level	2T	χ_4^2	χ_3^2	Lower Limit		μ Table II-6	Upper Limit		Failure Rate % Per 1,000 Hrs. at Lower Limit	Failure Rate % Per 1,000 Hrs. from Table II-6
				Hours	Months		Hours	Months		
99	752,640	34,267	4.075	21964	30.4	23,800	184,697	256.5	4.6%	4.2%
95	752,640	28.845	5.629	26093	36.2	28,500	133,708	185.7	3.8%	3.5%
90	752,640	26.296	6.571	28622	39.8	32,000	114,540	159.1	3.5%	3.1%
60	752,640	20.465	9.467	36777	51.1	45,000	79,501	110.4	2.7%	2.2%
50*	752,640	15.338	13.339	49070	68.2	48,800	56,424	78.4	2.0%	2.0%

T = 376,320
k = 7
n = 18
μ = MTF from Table II-6 Reliability Calculator.
α = An assumed constant failure rate occurring between infant mortality and wear out failure.
χ_4^2 = 16 degrees of freedom
χ_3^2 = 14 degrees of freedom

*The results of the 50% confidence interval test are not considered significantly in error. The calibration of the circular slide and the rounding off of numbers would account for the difference of 270 hours.